High-Thermal-Conductivity, Mesophase-Pitch-Derived Carbon Foams: Effect of Precursor on Structure and Properties

James Klett, Rommie Hardy[†], Ernie Romine[‡], Claudia Walls , Tim Burchell

Carbon and Insulation Materials Technology Group, Metals and Ceramics Division,
Oak Ridge National Laboratory, Oak Ridge TN, 37831-6087

[†]Alabama A&M, P.O. Box 1432, Normal, AL 35762

[‡]Conoco Inc., 1000 South Pine, P.O. Box 1267, Ponca City, OK 74602-1267

ABSTRACT

Pitch-based carbon foams are not new, but the development of high thermal conductivity foams for thermal management applications has yet to be explored. The research reported here focused on a novel foaming technique and the evaluation of the foaming characteristics of two mesophase pitches (Mitsubishi ARA24 and Conoco Dry Mesophase). After graphitization to 2800°C, densities of the graphite foams ranged from 0.2 to 0.6 g/cm^3, with average pore diameters ranging from 275 μm to 350 μm for the ARA24-derived foams, and from 60 μm to 90 μm for the Conoco-derived foams. Scanning electron microscopy and polarized light optical microscopy were performed to characterize the cell walls, revealing highly aligned graphitic-like structures along the axis of the ligaments. Analysis of x-ray diffraction results determined that the foams exhibited average interlayer (d_{002}) spacings as low as 0.3355 nm, stack heights (L_c) up to 80 nm and crystallite sizes (L_a) up to 20 nm. Finally, thermal diffusivity measurements were performed revealing that the bulk thermal conductivity varied with density from 40 to 150 W/m· K. The specific thermal conductivities of the graphitized foams were more than six times greater than solid copper.

KEY WORDS: A. graphite, mesophase pitch B. graphitization C. x-ray diffraction
D. thermal conductivity

1. Introduction

Contemporary advanced structural composites exploit the extraordinary mechanical properties of graphite [1] by creating a disconnected network of graphitic filaments held together by an appropriate matrix binder. Recently, the extraordinary thermal properties of graphite fibers have been exploited in a similar manner for thermal management applications. However, like the mechanical properties, the high thermal conductivity of the resultant composites is limited to the direction of the fibers. In most affordable composites, (typically 1- or 2- directional (1D, 2D)) this results in very high in-plane thermal conductivities and relatively low thermal conductivities in the out-of-plane (through thickness) direction (as seen in Table I [2-5]). This is because, in the out-of-plane direction, the matrix is the dominant phase for heat transfer. Even when carbon is the matrix, it typically does not develop the unique orientation found along the axis of carbon fibers (a result of the extension during spinning). This, combined with the tortuous path of heat transfer around voids, fibers, and matrix cracks, results in low out-of-plane composite thermal conductivity. Unfortunately, this can be a limiting factor in many heat sensitive applications ranging from wing leading edges, to electronic packaging, and heat exchangers.

Mesophase pitch-derived carbon foam, on the other hand, can be considered as an interconnected network of graphitic ligaments and, thus, should exhibit isotropic material properties [6, 7]. Hence, foams represent a potential reinforcing phase for structural composite materials and potentially, a cheaper alternative to carbon fibers. More importantly, graphite foam-based composites would be expected to exhibit higher out-of-plane thermal conductivities than typical 1-D or 2-D carbon fiber reinforced composites because of the continuous graphitic network.

In recent years the use of carbon fibers has evolved from structural reinforcement to a thermal management material, with the emphasis in applications such as high-density electronic modules,

communication satellites, and automotive systems. The primary concerns in thermal management applications are high thermal conductivity, low weight, low coefficient of thermal expansion and low cost [8]. Such applications have focused on sandwich structures (a high thermal conductivity material encapsulating a structural core material) to provide the required mechanical properties [8]. However, since structural cores (e.g. honeycombs) are typically low-density materials, the thermal conductivity of the overall composite through the thickness is relatively low (~3-10 W/m· K for aluminum honeycomb [4, 9]). Metallic foams are being explored as a potential core material; however, the thermal conductivities are still low, 5 - 50 W/m· K [9] and are not greater than typical carbon-carbon composites (see Table I). Existing carbon foams are typically reticulated glassy carbon foams with a pentagonal dodecahedron structure [10, 11, 12], illustrated in Figure 1, and exhibit thermal conductivities less than 1 W/m· K [9, 13, 14, 15]. The pitch-derived graphitic foams reported here exhibit a spherical morphology, and present a unique solution to this problem by offering high thermal conductivity with a low weight.

If a mesophase pitch is used as the precursor, well ordered structures will be formed in the ligaments [6, 16, 17], which should lead to improved thermal conductivity with appropriate post processing. Typical foam forming processes utilize a blowing technique, or pressure release, to produce foam of the pitch precursor [16, 18-21]. As the bubbles in the foam grow, bi-axial extension orients the mesophase domains parallel to the cell walls, similar to the uni-axial extension during melt extrusion (or spinning) of mesophase pitch-based carbon fibers. As with carbon fiber production, the pitch foam is then stabilized by heating in air or oxygen for many hours to cross-link the structure, and "set" the pitch, so it does not melt during further heat treatment [18, 22]. Stabilization can be a very time consuming and expensive process depending on the part size. The "stabilized" pitch foam is carbonized in an inert

atmosphere to temperatures as high as 1100°C, producing a structural material suitable for composite reinforcement [7, 16, 18-22].

A new, less time consuming process for fabricating pitch-based graphitic foams without the traditional blowing and stabilization steps, has been developed at Oak Ridge National Laboratory (ORNL) and is the focus of this research. It is believed that this new foam will be less expensive and easier to fabricate than traditional foams since the time consuming oxidative stabilization step has been removed. Potentially, the process will lead to a significant reduction in the cost of carbon-based thermal management and structural materials (i.e. foam-reinforced composites and foam core sandwich structures).

2. Experimental

2.1 Foam Processing

In this research, two mesophase pitches were used to produce graphitic foam: Mitsubishi ARA24 naphthalene-based synthetic pitch, and a proprietary mesophase pitch from Conoco Inc. labeled Conoco Dry Mesophase. The properties of each pitch are listed in Table 2. Four different operating pressures (A < B < C < D) were used to produce foam with a range of densities, pore structures, and thermal properties. All foam samples were carbonized at 0.2°C/min to 1000°C and then graphitized at 10°C/min in Argon to 2800°C with a 2-hour soak at temperatures.

2.2 Foam Characterization

The average pore diameter and pore distribution were measured using optical image analysis with a Nikon Microphot-FXA microscope and digital capture equipment. In order to develop a fundamental understanding of the foam structure and graphitic morphology, several other examination techniques

were employed: Optical microscopy with cross-polarized light and a quarterwave retarder was performed on a Nikon Microphot-FXA microscope; samples were examined using a JOEL scanning electron microscope; and the thermal conductivity, κ, of the foam was determined with a xenon flash diffusivity technique. The thermal diffusivity, α, was first measured on samples 12-mm diameter by 12-mm thick on a custom built machine in the High Temperature Materials Laboratory at Oak Ridge National Laboratory. The sample density, ρ, and specific heat capacity, C_p, (assumed to be 713 J/Kg· °C [23]) were then used to calculate the thermal conductivity with the following relation:

$$\kappa = \alpha \cdot \rho \cdot C_p.$$

Finally, the same foam samples used for thermal diffusivity were machined to cylinders 12-mm diameter by 6-mm thick for x-ray diffraction studies. Room temperature X-ray diffraction measurements were conducted using a Scintag PAD V vertical $\theta/2\theta$ goniometer. The diffractometer utilized CuKα radiation (45 kV and 40mA) and a Si(Li) Peltier-cooled solid state detector. The data were collected as continuous scans, with a step size of 0.02 °2θ and a scan rate of 1 °2θ/minute between 10 and 90 °2θ. Since a completely random orientation of the crystallites is already present in the foam, powdering was not necessary.

Lattice spacing was determined from the indexed diffraction peak positions [24]. The 002 and 1010 diffraction peak breadths were analyzed using the Scherrer equation to determine the crystallite dimensions in the a- and c- directions:

$$t = \frac{\mathbf{0.89}\,\lambda}{B\cos(\mathbf{2}\theta)},$$

where t is the average crystallite size in the sample, λ is the X-ray wavelength (1.540562 Å), B is the breadth of the diffraction peak (full width half maximum (FWHM) minus the instrumental breadth, 0.06°), and 2θ is the diffraction angle.

3. Results and Discussion

3.1 Processing

It was found that during processing into foam, the carbon yields of the pitches, presented in Table 3, improved over that measured at atmospheric pressure listed in Table 2. The carbon yield of the ARA24 pitch increased significantly from 78 % at 1000°C to 86 % while the carbon yield of the Conoco pitch changed only slightly, however, from 87 % to 88 %. Table 4 presents the apparent densities of the foams after foam production and subsequent heat treatments. As expected, the Conoco pitch yielded foams with higher densities than foams produced with the ARA24 mesophase pitch. Since the higher melting temperature of the Conoco pitch should yields higher viscosities during processing [25], it is reasonable to expect smaller bubble sizes in the Conoco-derived foams compared to ARA24-derived foams processed at similar conditions.

3.2 Microstructural Characterization

3.2.1 Cell Sizes. Figure 2 presents the average pore diameters ($\bar{x}$) and the standard deviation (σ) for both ARA24 pitch and Conoco pitch-derived foams as a function of density. The ARA24 pitch-derived foams exhibited a larger mean pore size than the Conoco pitch-derived foams. However, the ARA24 pitch-derived foams exhibited a smaller relative distribution ($\sigma/\bar{x}$) than the Conoco-derived foams. The pore distribution of the foams produced from the Conoco pitch is heavily skewed to smaller pore sizes.

It was surprising that the average pore sizes of either foam did not show any statistical change with density. It is important to note that due to the larger pore sizes in the ARA-derived foams, significantly fewer bubbles were counted with the optical image analysis equipment (250 as compared to 2000 for

the Conoco-derived foams). This reduced data set could result in errors. Also, the ARA-derived foams exhibit a slight density gradient from the bottom of the foam to the top, due to gravity and the low viscosity during processing. While care was taken to minimize these effects in the measured samples, it is possible that the samples of the ARA-derived foams used for image analysis were not machined from consistent locations, resulting in insufficient sampling of the bubble population to provide a statistically sound basis for analysis. Additional characterization is ongoing in order to expand the available data set.

3.2.2 Pore Morphology. Figures 3-9 are scanning electron micrographs of fracture surfaces revealing the pore structure of the Mitsubishi ARA24 and Conoco-derived foams heat-treated at 1000°C and 2800°C. Both foams exhibit a spherical structure with open, interconnected pores between most of the cells (P1 and P2 in Figure 3). It is evident from the images that the graphitic structure is oriented parallel to the cell walls and highly aligned along the axis of the ligaments (L in Figures 3, 6 and 8). In fact, this feature is striking since it is clearly visible in foams with a final heat treatment of only 1000°C (Figure 6). This highly aligned structure is significantly different from typical vitreous carbon foams: vitreous carbon foams are void of graphitic structure, have large openings and linear ligaments, and are mostly pentagonal dodecahedron in shape (Figure 1). Figures 7 and 9 are SEM images of the foams after graphitization at 2800°C. Although it is evident that the foams are highly graphitic, they are more disordered and not as spherical after graphitization. The cells also contain more extensive layering due to shrinkage during heat treatment. The extended graphitic structure of the foams will impart excellent thermal properties once they are graphitized.

Figures 5, 8, and 9 show that the Conoco pitch-derived foam has a strikingly different structure. First, the cells are significantly smaller and the cell size does appear to change slightly with density. Although the foam is open celled, the openings are fewer in number compared to the foams produced from the Mitsubishi ARA24 pitch. This suggests that the cells in the Conoco-derived foams do not have openings to as many neighboring cells as those in the ARA24-derived foams.

3.2.3 Cells Walls

At first inspection, the structure and geometry of the Mitsubishi ARA24-derived foams (Figure 3, 4, 6 and 7) appear to vary little with density. However, after closer inspection it appears that the junctions (J in Figures 3 and 6) get progressively smaller with decreasing density (A < B < C < D). Moreover, it can be seen that in the junctions between ligaments, the graphitic structure is less aligned and possesses more folded texture. It is postulated that this arises from the lack of stresses at this location during forming. During bi-axial extension of the walls during bubble growth, there exists high stresses along the bubble walls, causing the molecules to align along the walls. However, in certain regions (junctions between ligaments), the stresses are minimal, and therefore, little rearrangement of the mesophase occurs. Hence, the graphitic structure in these regions is primarily an artifact of the structure in precursor mesophase prior to pyrolysis and polymerization.

Like the ARA24-derived foams, the ligaments in the Conoco-derived foams contain highly aligned graphitic structures (L in Figure 5 and 8). Also, it appears that the junctions (J in Figure 8) between the ligaments are less disrupted than that found in the ARA24 foams. The graphitic structure appears to extend from the ligaments through the junctions. It is unclear whether this is due to the smaller cell size in the Conoco pitch foam or is attributable to the nature of the precursor mesophase (melting point, viscosity, molecular structure, etc.). It should be noted that the ARA24 mesophase molecules are more

rod like [26] in nature and the Conoco mesophase (being a petroleum derivative) is more disc-like (Figure 10) [27]. The differences in chemical reactivity, degree of aromaticity, and molecular weight of the pitch molecules could affect the viscosities during processing. These differences in viscosity could contribute to differences in behavior (response) to stretching during the bubble formation and growth stage and, ultimately, affect the cell structures developed.

3.2.4 Cell Openings

It can be seen in both the ARA24 and Conoco-derived foams (Figures 3-9) that the openings between cells are of two types. The first type of opening is smooth and circular (P2 in Figure 3, 6 and 8) and forms while the pitch is fluid. The second type of opening appears to have formed by brittle fracture of the cell walls after the pitch hardened (coked) (P1 in Figure 3). This fracture can occur during the later stage of the foaming step, after pitch hardening (>500°C) or during post foaming heat treatments. The ARA24-derived foams with lower densities (A) appear to exhibit more shattered openings rather than smooth openings, indicating that more cells were opened during further heat treatment. In the foams produced from Conoco pitch, there appear to be very few fractured openings compared to the ARA24 pitch-derived foams. The reasons for this remain unexplained at this time. The differences in cell openings will, ultimately, affect permeability through the foam that, in turn, will affect efficiencies in porous media heat transfer devices developed with the foam.

3.2.5 Microcracking

Foams with lower densities (process A) appear to exhibit more microcracks (M in Figure 3), probably because of the thinner walls exhibited by these foams. After graphitization (M in Figure 4) the foams exhibit even more microcracking that is predominantly between the basal planes. The high content of microcracking will adversely affect mechanical properties. However, it is expected that the

microcracks will not significantly affect thermal properties because of their alignment parallel to the basal planes.

3.2.6 Microstructure Development

The growth and mobility of the mesophase domains is strongly influenced by the viscosity of the mesophase during processing. While the pitch is fluid (during the bubble growth stage), the mesophase domains will orient in response to the stresses resulting from bi-axial extension in the walls of the foam. Hence, the mesophase domains orient parallel to the surface of the bubbles. As the bubbles join and openings between the bubbles develop, a strut-like morphology develops with the orientation in the surface of the bubbles translating to the ligaments, yielding highly aligned mesophase domains along the axis of the ligament. During this development, a lower viscosity will result in better re-orientation due to extension, thus resulting in enhanced alignment of the mesophase domains parallel to the axis of the ligaments. Alignment of the mesophase will translate to better alignment of the graphitic crystal after heat treatment and, consequently, improved thermal properties. Therefore, a sufficiently low viscosity is required during bubble growth to achieve ideal alignment of the mesophase domains along the ligaments of the foam.

Last, mesophase growth (enlargement rather than alignment) is also an important mechanism by which pitch-derived carbons exhibit enhanced graphitic properties (thermal conductivity, stiffness, etc.) and is detailed elsewhere [28-30]. Domain growth occurs when the pitch is fluid and the domains have sufficient mobility to grow and coalesce [26-28]. Domain growth is important since it translates to larger graphitic crystals and fewer domain boundaries in the material after graphitization (properties which will improve the thermal conductivity). As in the orientation mechanism, a higher viscosity will inhibit molecule mobility, thus restricting growth and coalescence of the mesophase domains during

processing. The reduced mobility and mesophase domain size growth is also seen in the process of oxidative stabilization of mesophase carbon fibers and other mesophase pitch foams. Because of the lower viscosity of the ARA24 mesophase pitch during processing, it is expected that the ARA24 mesophase pitches will yield foams with better alignment and larger crystal sizes than that exhibited in foams produced from the Conoco mesophase.

3.2.7 Optical Microstructure.

Figures 11 and 12 are optical micrographs of the Mitsubishi ARA24 pitch-derived foams under cross-polarized light with a quarterwave retarder. The micrographs reveal that the graphene layer planes are highly oriented parallel to the surface of the bubbles and along the axis of the ligaments, indicated by the monochromatic regions (MC) in Figures 11. Large fold lines are visible in the thicker cell walls (ligaments), evidence of very large ordered structures parallel to the cell walls. The lack of an oxidative stabilization allows the mesophase domains to grow very large during the processing, producing very few domain boundaries in the ligaments. The large optical domains that result are even evident in the pictures of the foams heat-treated to only 1000°C (Figures 11 and 12). The mesophase alignment is predominantly parallel to the surface of the bubbles, with a disruption of the alignment in the junctions (J in Figure 12). When the samples are graphitized, the alignment in the ligaments becomes more refined while the mesophase in the junctions becomes very folded. The multicolored regions in the high magnification images of the junctions between ligaments in the Mitsubishi ARA24 foams, (J in Figure 12) confirm that although the region is graphitic, there is more fold-sharpening and random orientation of the crystals in these regions than that found in the ligaments. These regions will serve to reduce the overall thermal conductivity (because of their increased thermal resistance compared to the ligaments), although the foam should still exhibit excellent thermal conductivity.

It is noted that in Figure 11, all the microcracking (M) appears to run parallel to the basal planes, similar to that observed with SEM imaging. These microcracks most likely arose during heat treatments as the structure shrinks due to the reduction in interlayer spacing and the increase in real density. Table 5 presents the skeletal density changes of the ARA24-derived foams at different stages of processing. As can be seen, the density of the graphite structure changes significantly with heat treatment and an ultimate density of 2.23 g/cm^3 is achieved in the structure of the ARA24-derived foams.

Comparison of Figure 11 A through D clearly indicates that the cell wall thickness changes dramatically with density in the ARA24 derived foams. Therefore, the apparent density of the ARA24-derived foams appears primarily to depend on the thickness of the cell walls.

An examination of the Conoco pitch-derived foams (Figures 13 and 14) reveals monochromatic regions (MC) in the ligaments. This suggests that the Conoco pitch-derived foams exhibit a highly aligned graphitic structure along the axis of the ligaments, similar to the ARA24-derived foams, indicating that the foam should exhibit good thermal conductivity. However, images of the junctions in the lower density foams (J in Figures 13 and 14) suggest that the Conoco-derived foams contain better orientation of the mesophase in these regions (fewer multicolored regions). The flow domains in the Conoco-derived foams appear to extend from the ligament through the junctions to the next ligament. The appearance of many junctions without significant disruption (see J in Figure 15), is likely due to the fact that the junctions in the ARA24-derived foam are larger in size than the Conoco-derived foams.

The Conoco pitch-derived foams (Figure 14 A through D) exhibited a similar variation of cell wall thickness with density as that found in the ARA24 pitch-derived foams. However, the effect is not as marked as with the ARA24 foams.

As found in the ARA-derived foams, the microcracks in the Conoco-based foam (M in Figures 13 and 14) are primarily separations between the graphitic planes. These types of cracks will serve to weaken the foam structurally, but should not significantly interfere with the thermal transport properties.

3.3 Thermal Diffusivity

The validity of the flash diffusivity method and whether the open porosity would permit penetration of the heat pulse into the sample, thereby invalidating the test, had to be established. Deep penetration of the pulse in samples typically causes a change in the characteristic heat pulse on the back face of the sample. Thus, errors in the reported diffusivity can be as high as 20% [31, 32]. However, the rather large ligaments and small openings of the foam limits the depth of penetration to about two pore diameters (less than 800 μm), or less than 6% penetration. Therefore, it was believed that this technique would yield a fairly reasonable value for the thermal diffusivity. This was confirmed by testing samples in which the non-porous skin produced during formation was left on the surface of the test sample. This surface was placed facing the heat pulse, thereby preventing any penetration of the pulse into the sample. The measured diffusivities (between samples with and without a surface skin) varied by less than five percent, verifying the flash method as a viable method to measure the thermal diffusivity of these foams. For foams with large openings, such as reticulated polymer or pitch-derived foams, excessive penetration of the thermal pulse would render this technique unreliable.

The thermal conductivity of the carbonized foams (Figure 16) was, as expected, very low (1-2 W/m· K) which is consistent with other porous carbon materials [7, 16, 19, 21, 33-36]. The thermal conductivity of the graphitized ARA24 foam ranged from 50 to 150 W/m· K and the thermal conductivity of the Conoco-derived foams exhibited thermal conductivities ranging from 40 to 135

W/m· K (presented in Figure 17). This is remarkable for a material with such a low density, 0.27 to 0.57 g/cm^3. Linear regression of the data for both foams shows that the Conoco-derived foams exhibits a marginally lower thermal conductivity (with 95% confidence intervals), compared to the AR-derived foams. This might be explained by the differences in molecular structure of the starting precursor materials (as discussed in section 3.2.6) that might yield slightly different crystal lattice structures. Petroleum-derived pitches also contain more impurities and infusibles than the synthetic ARA24 mesophase pitch and, therefore, may develop more lattice imperfections than synthetic pitches that, unfortunately, would be too small to observe in optical micrographs.

The foam exhibits isotropic thermal conductivities comparable to the in-plane thermal conductivity of other thermal management materials and significantly higher than in the out-of-plane directions (Table 6). Although several of the other thermal management materials have higher in-plane thermal conductivities, their densities are much greater than that of the foam. Hence, the specific thermal conductivity of the foam is significantly greater than most of the available thermal management panels (in-plane and out-of-plane). In fact, the specific thermal conductivity is more than six times greater than copper and five times greater than aluminum, the preferred materials for heat sinks.

It is clear that for weight sensitive thermal management applications or applications where transient conditions occur often, the graphitic foam can be superior in thermal properties to other available materials. The advantage of isotropic thermal and mechanical properties combined with open celled structure should allow for novel designs that are more design flexible and efficient.

3.4 X-ray Analysis

Figure 18 is the x-ray diffraction spectra for a graphitized foam produced from Mitsubishi ARA24 mesophase pitch. The 002 peaks (which are characteristic of interlayer spacing) in Figure 18 are very

narrow and asymmetric, indicative of highly ordered graphite. The 002 and 004 peaks get narrower and more intense with increasing density, as expected with a larger sampling mass. The interlayer spacings calculated with the Scherrer equation ranged from 0.3364 nm to 0.3355 nm and decreased as a function of density and is presented in Table 7. The interlayer spacing found in the higher density foam (Process D), 0.3355 nm, was significantly closer to pure graphite, 0.3354 nm, than that found in most high performance pitch-derived carbon fibers, 0.3366 nm [37]. Table 8 is a comparison of x-ray diffraction results of the graphite foam and various high performance carbon fibers [37].

The crystallite size in the c-direction (L_c) ranged from 46.6 to 82.4 nm, and the crystallite size in the a-direction (L_a) calculated from the 100 peak (or $10\bar{1}0$ in hexagonal nomenclature) ranged from 11.8 to 21.5 nm. These crystallite sizes are similar to typical high thermal conductivity carbon fibers such as K1100 and vapor grown carbon fibers (VGCF) [37-39] and, therefore, the high thermal conductivity measured for the foams is not unreasonable. In fact, the d-spacing is better than VGCF, which have exhibited thermal conductivities as high as 1950 W/m· K [37]. Katzman et. al. [33] illustrate a direct relationship of thermal conductivity to d-spacing indicating that fibers with d-spacings of between 0.3355 to 0.3360 nm should exhibit thermal conductivities between 1500 and 2000 W/m· K. Hence, the ligaments, or cell walls, of the foam should exhibit thermal conductivities greater than 1500 W/m· K.

Although the Conoco B pitch-derived foam had similar x-ray data (Figure 19), the intensities were not as large as those for the Mitsubishi ARA24-derived foams. The stack heights (L_c) and crystal size (L_a) of the Conoco-derived foams were similar to the ARA24-derived foams. However, the interlayer spacing (d_{002}) did not follow a decreasing trend with increasing density as that found in the Mitsubishi ARA24 foams, although the interlayer spacings were all smaller than that found in high performance carbon fibers.

The fact that the crystal parameters in both foams are so close to perfect graphite is remarkable because x-ray diffraction results are averages over the entire sample. It should be noted here that measurement of interlayer spacing and lattice parameters is difficult and the trends (or lack of them) seen in the foams may be coincidental, and therefore specific conclusions about thermal properties cannot be drawn. However, several important statements can be made. First, the extremely low interlayer spacings confirm other analysis techniques that indicate the foam is highly graphitic and the ligaments contain graphitic alignment as good as (if not better than) traditional high thermal conductivity carbon fibers. Second, with L_a and L_c sizes comparable to high performance carbon fibers, it is reasonable to expect that the ligaments will exhibit extremely high thermal conductivities as well.

3.5 Foam-based Structures

Several foam core sandwich panels were fabricated by laminating the foam with aluminum and copper facesheets (0.5-mm thick). The isotropic thermal conductivity of these foam-core composites (see Figure 19) should provide thermal management characteristics comparable to existing materials. This should lead to more efficient thermal management materials and, possibly, a new approach to thermal management. Also, successful densification with aluminum, carbon, epoxy, and thermoplastic resins has been accomplished, demonstrating the use of foam as the reinforcement in a composite structure where high thermal conductivity is required, but at a lower cost than traditional high conductivity carbon fibers.

4. Conclusions

The manufacture and properties of high thermal conductivity carbon foams have been reported. It was shown that pitch precursor characteristics can affect foam structure and properties such as bubble size and ligament structure. It was found that a pitch with a lower melting point would produce foams with larger pore sizes. However, the resulting thermal conductivity was relatively unaffected by precursor characteristics. On the other hand, processing variables, such as operating pressure and heat treatment temperature, showed a large effect on bubble size and, more importantly, thermal properties of the foams. Hence, the graphitic characteristics of the foam, such as lattice parameters, thermal conductivity, etc, appear rather insensitive of the precursor mesophase material, compared to operating pressure and heat treatment temperature.

The existence of very sharp 002 and $10\bar{1}0$ peaks confirms that the graphitic crystals are very large and are highly oriented. Under cross-polarized light, very large monochromatic regions in the ligaments of the foam are visible, suggesting that these ligaments will behave similar to high thermal conductivity carbon fibers, such as K1100 and VGCF. These properties, combined with the continuous graphitic network throughout the foam (unlike carbon fiber reinforced composites), result in an isotropic bulk thermal conductivity as high as 150 W/m· K and a specific conductivity up to 6 times that of copper, an industry standard for thermal management.

Although the data and discussion presented in this paper illustrate the potential of this material to be an enabling technology for many applications, further work is needed. It is believed that through process optimization (the elimination of cracks and development of better orientation in the junctions) thermal conductivities of the foams could be improved. A full characterization of the kinetics of the foaming reaction should be undertaken in order to allow optimization of the process. Finally, the effects

of bubble openings and heat treatment conditions on the mechanical and thermal properties should be evaluated.

5. References

1. Edie, DD. In: Figueiredo, J. L., et. al., editor. Carbon Fibers, Filaments, and Composites, Kluwer Academic Publishers, 1990:43-72.

2. Olhlorst CW, Vaughn WL, Ransone PO, Tsou H-T. Thermal Conductivity Database of Various Structural Carbon-Carbon Composite Materials. NASA Technical Memorandum 4787, November 1997.

3. Amoco Product Literature, 1997.

4. Hexcel Product Data Sheet, 1997.

5. Steiner K, Banhard J, Baumister J, Weber M. Extended Abstracts, 4th International Conference on Composites Engineering, Kona, (Hawaii, USA), July 6-12, 1997: 943-944.

6. Hagar JW Lake ML, Mat. Res. Soc. Symp. 1992;270:29-34.

7. Hagar JW, Mat. Res. Soc. Symp. 1992;270:41-46.

8. Shih, W. Development of Carbon-Carbon Composites for Electronic Thermal Management Applications. IDA Workshop, May 3–5, 1994.

9. Gibson LJ, Ashby, MF. Cellular Solids: Structures & Properties, Pergamon Press, New York, 1988.

10. Glicksman LR, Torpey M. Proceedings of the Polyurethane World Congress, Aachen, Germany, 1987.

11. Glicksman LR, Marge AL, Moreno JD. Developments in Radiative Heat Transfer, ASME HTD – 1992;203.

12. Kuhn J, Int. J. Heat Mass Transfer 1992;35(7):1795-1801.

13. Glicksman, LR, Schuetz M, Sinofsky M. A Study of Radiative Foam Heat Transfer through Foam Insulation. Report prepared by Massachusetts Institute of Technology under subcontract No. 19X-09099C, 1988.

14. Ultramet Product Literature, 1998.

15. Doermann D, Sacadura JF. J. of Heat Transfer 1996;118:88-93.

16. Sandhu SS, Hagar JW. Mat. Res. Soc. Symp. 1992;270:35-40.

17. White JL, Sheaffer PM, Carbon 1989;27(5):697-707.

18. Bonzom A, Crepaux AP, Moutard AM. Process for preparing pitch foams and products so produced, The British Petroleum Company, U. S. Patent. 4276246, 1981.

19. Knippenberg, WF, Lersmacher B, Phillips Tech. Rev. 1976;36(4):93-103.

20. Aubert, JH, Mat. Res. Soc. Symp. 1990;207:117-127.

21. Cowlard FC, Lewis JC, J. of Mat. Sci. 1967;2:507-512.

22. Kearns K, The 21st Annual Conference on Ceramic, Metal, and Carbon Composites, Materials, and Structures, Cocoa Beach, Florida, 1997;835-847.

23. ASTM, vol. 15.01, C-781-96, 1999.

24. Klug HP, Alexander LE, X-Ray Diffraction Procedures for Polycrystalline and Amorphous Materials, 2nd edn., J. Wiley, New York, USA, 1974.

25. Nazem, FF. Carbon 1982: 20(4): 345.

26. Mochida, I. Carbon 1990;28(2):311-319.

27. Fitzer E, Carbon Fibers and Their Composites, Springer-Verlag, New York, New York, 1985.

28. Brooks JD, Taylor GH, "The Formation of Graphitizable Carbons from the Liquid Phase," Carbon 1965;3(2):185-199.

29. Zimmer JE, and White JL, Advances in Liquid Crystals 1982;5:157.

30. Rouzaud JN, and Oberlin A, Carbon 1989;27(4):517-529.

31. Inoue K, High Temp. Tech. 1990;8(1):21-26.

32. Cowan RD, J. of App. Phys. 1962;34(4):926-927.

33. Adams PM, Katzman HA , Rellick GS, Stupian. Carbon 1998:36(3): 159-318.

34. ERG product literature, 1998.

35. Dinwiddie RB, Nelson GE, Weaver CE. Proceedings 23rd Int. Thermal Conductivity Conference, Technomic Pub. Co., Lancaster PA, 1996:466-477.

36. Wei GC, and Robbins JM. Ceramic Bulletin 1985;64(5):691-699.

37. Lake M, Mat. Tech. 1996;11(4):131-144.

38. Jones SP, Fain CC, and Edie DD, Carbon 1997;35(10):1533-1543.

39. Brito K, Anderson DP, Proceedings of the 34th International SAMPE Symposium, 1989;34(1):190.

Acknowledgements

The authors wish to thank Conoco Inc. for supplying the proprietary pitches for this research, Claudia Rawn of ORNL for performing the x-ray analysis of the foams and Marie Williams of ORNL for SEM and optical analysis of the foams.

Research sponsored by the U.S. Department of Energy, Assistant Secretary for Energy Efficiency and Renewable Energy, Office of Transportation Technologies, as part of the Advanced Automotive Materials Program, under Contract No. DE-AC05-96OR22464 with Lockheed Martin Energy Research Corporation.

Table 1. Thermal properties of carbon fiber composites and other thermal management materials.

Material	Specific Gravity	Thermal Conductivity		Specific Thermal Conductivity*	
		In-plane	Out-of-plane	In-plane	Out-of-plane
		[W/m· K]	[W/m· K]	[W/m· K]	[W/m· K]
Typical 2-D Carbon-Carbon [2]	1.88	250	20	132	10.6
EWC-300/Cyanate Ester [3] Resin	1.72	109	1	63	0.6
Copper [3]	8.9	400	400	45	45
Aluminum [3]	2.77	150	150	54	54
Aluminum Honeycomb [4]	0.19	--	~10	--	52
Aluminum Foam [5]	0.5	12	12	24	24

* Defined as thermal conductivity divided by specific gravity.

Table 2. Properties of mesophase pitches used to produce graphitic foam.

Mesophase	**Softening Point [°C]**	**Mesophase Content [%]**	**Carbon Yield @1000 °C, N_2 [%]**
Mitsubishi ARA24	237	100	78
Conoco Dry Mesophase	355	100	87

Table 3. Pitch carbon yields during processing into foams with ORNL process.

	Cumulative Pitch Carbon Yields During Process D		
Mesophase	**630°C**	**1000°C**	**2800°C**
Mitsubishi ARA24	89.4 %	86.2 %	85.9 %
Conoco	92.6 %	88.7 %	88.3 %

Table 4. Density of foams produced at different operating conditions after carbonization and graphitization.

Process	Bulk Density [g/cm^3]			
	ARA24		Conoco	
	1000°C	2800°C	1000°C	2800°C
A	0.22	0.25	0.33	0.35
B	0.37	0.39	0.40	0.40
C	0.44	0.48	0.49	0.49
D	0.54	0.57	0.56	0.59

Table 5. Skeletal density changes of ARA24-dervied foams at different stages of processing measured by Helium Pycnometry.

Heat Treatment Temperature	**Density**
[°C]	*[g/cm^3]*
630	1.44
1000	2.06
2800	2.23

Table 6. Thermal properties of the pitch-derived carbon foams compared to other thermal management materials.

Material	Specific Gravity	Thermal Conductivity		Specific Thermal Conductivity*	
		In-plane	Out-of-plane	In-plane	Out-of-plane
		[W/m· K]	[W/m· K]	[W/m· K]	[W/m· K]
ARA24-derived foam - D	***0.57***	***149***	***149***	***261***	***261***
Conoco-derived foam - D	***0.59***	***134***	***134***	***227***	***227***
Typical 2-D Carbon-Carbon [2]	1.88	250	20	132	10.6
EWC-300/Cyanate Ester [3] Resin	1.72	109	1	63	0.6
Copper [3]	8.9	400	400	45	45
Aluminum [3]	2.77	150	150	54	54
Aluminum Honeycomb [4]	0.19	--	~10	--	52
Aluminum Foam [5]	0.5	12	12	24	24

* Defined as thermal conductivity divided by specific gravity.

Table 7. Crystal parameters measured by x-ray diffraction.

Foam	Specific Gravity	Interlayer Spacing d_{002} [nm]	Crystal Size L_a [nm]	Stack Height L_c [nm]
Mitsubishi ARA24				
A	0.25	**.3364**	**11.8**	**48.2**
B	0.39	**.3362**	**17.8**	**46.6**
C	0.48	**.3360**	**21.5**	**79.3**
D	0.57	**.3355**	**18.4**	**82.4**
Conoco B				
A	0.35	**.3357**	**16.7**	**29.5**
B	0.40	**.3363**	**13.0**	**38.7**
C	0.49	**.3358**	**19.5**	**97.6**
D	0.59	**.3360**	**19.8**	**50.8**

Table 8. Comparison of x-ray diffraction results of various carbon fibers and the graphitic foam.

Material	Heat Treatment	Interlayer Spacing d_{002}	L_a	L_c	Estimated Ligament Conductivity
	[°C]	[nm]	[%]	[%]	[W/m· K]
Clemson Ribbon [36]	2400	.3369	62	19	950
K1100 [33]	3000	.3366	109	62	884
Experimental Pitch Fiber[33]	3000	.3364	102	66	1060
Fixed catalyst VGCF [35]	2800	.3366	40[37]	37[37]	1950
Conoco-D Foam	**2800**	**.3360**	**20**	**51**	**>1500**
ARA24-D Foam	**2800**	**.3354**	**18**	**82**	**>1500**

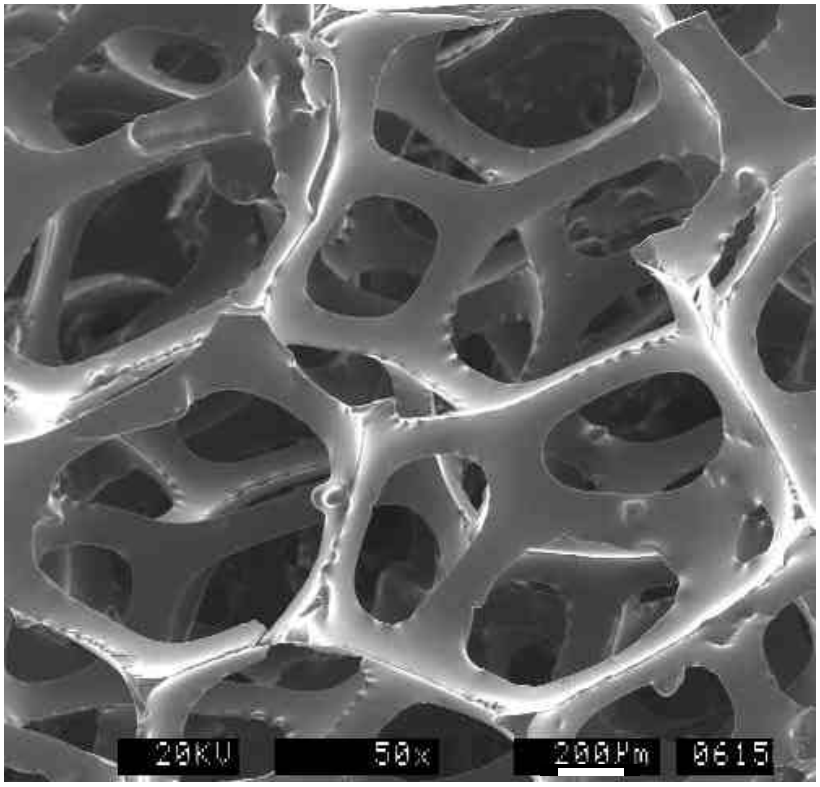

Figure 1. Typical reticulated glassy carbon foam produced by ERG Corporation.

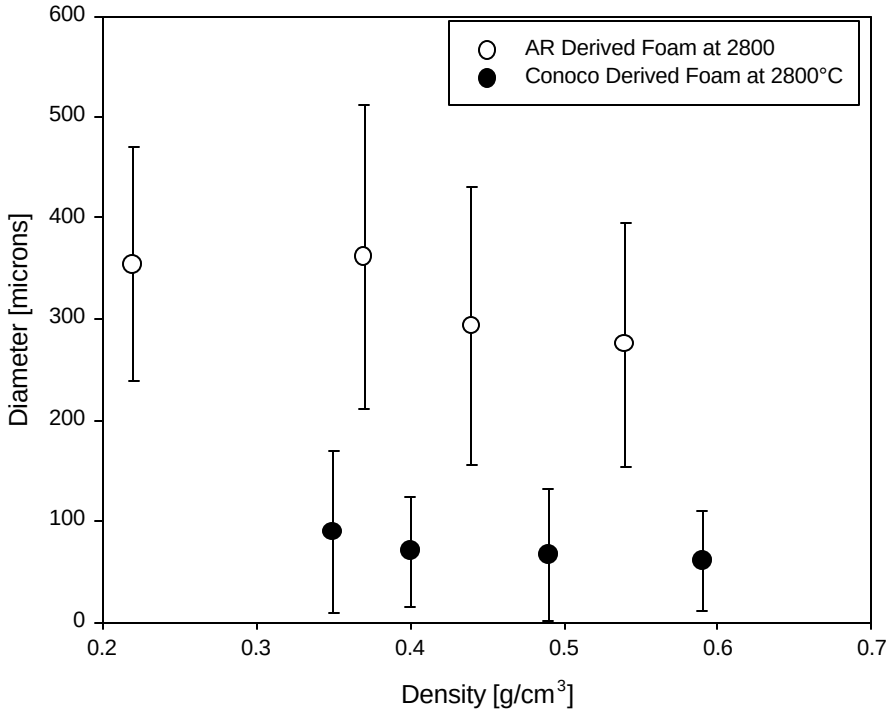

Figure 2. Mean pore diameter as a function of foam density [Error bars represent ± 1 standard deviation.

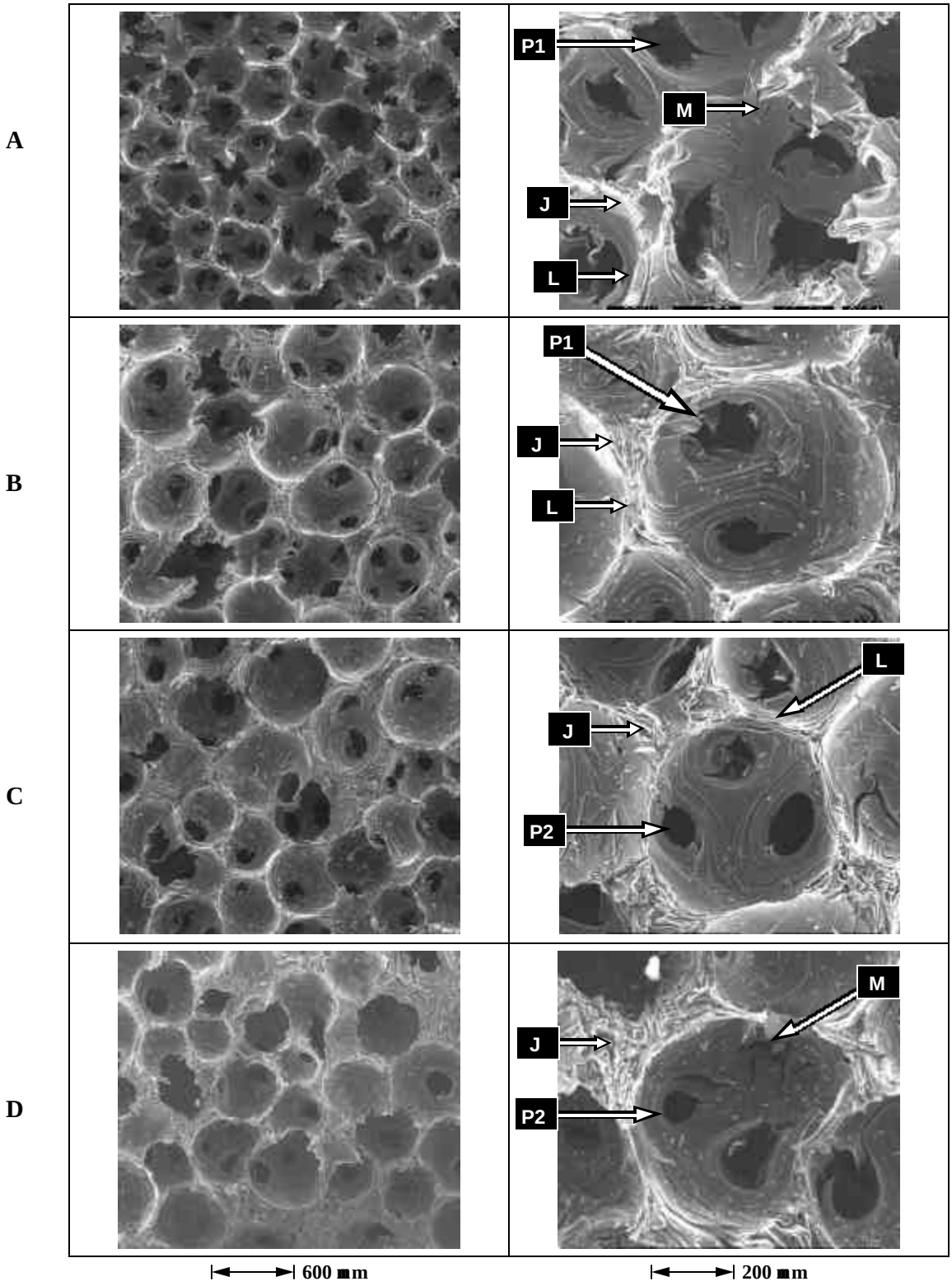

Figure 3. SEM photomicrographs of the foams produced from Mitsubishi ARA24 Pitch at different densities A < B < C < D (all samples carbonized at 1000°C).

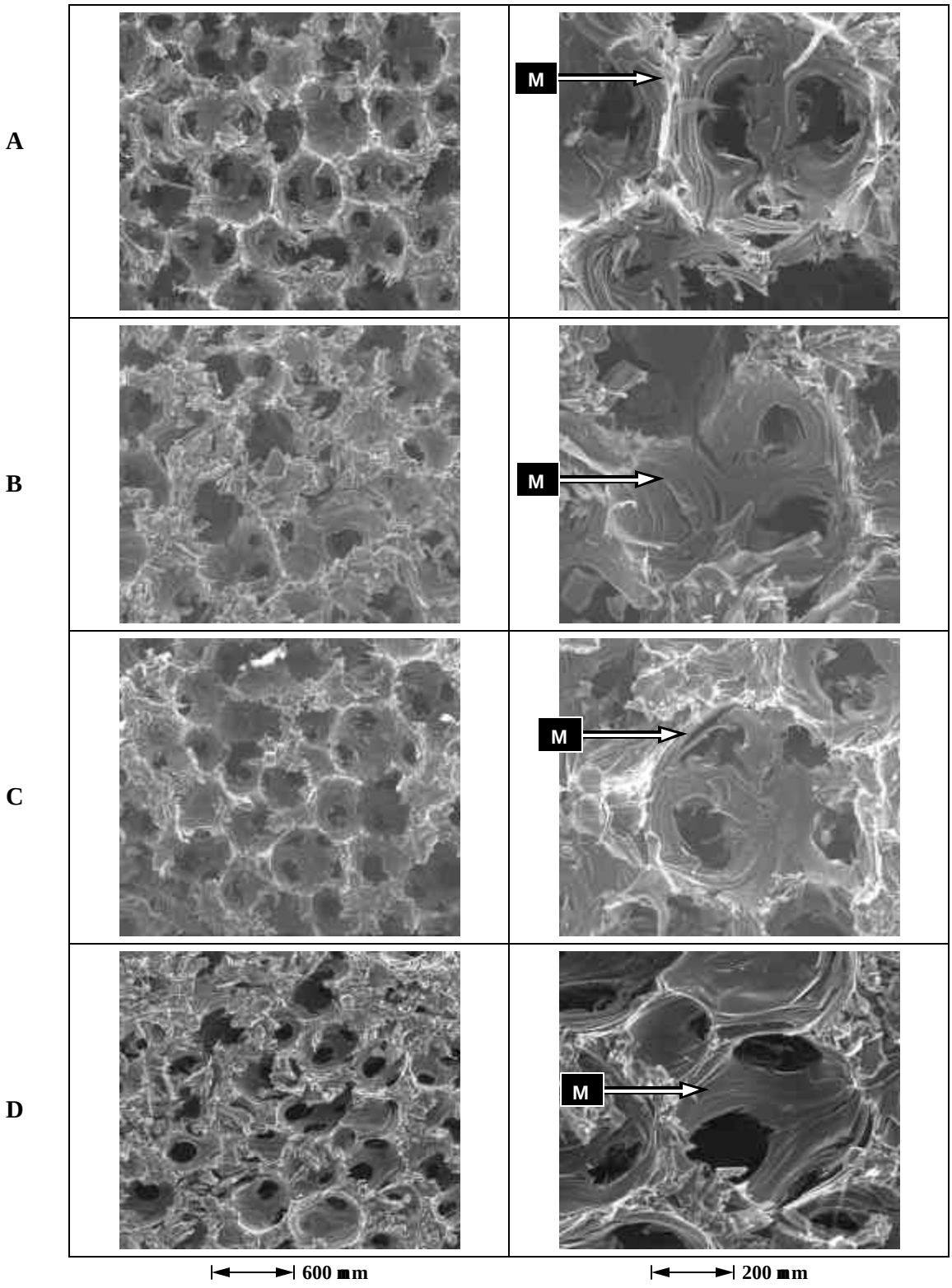

Figure 4. SEM photomicrographs of the foams produced from Mitsubishi ARA24 Pitch at different densities A < B < C < D (all samples graphitized at 2800°C).

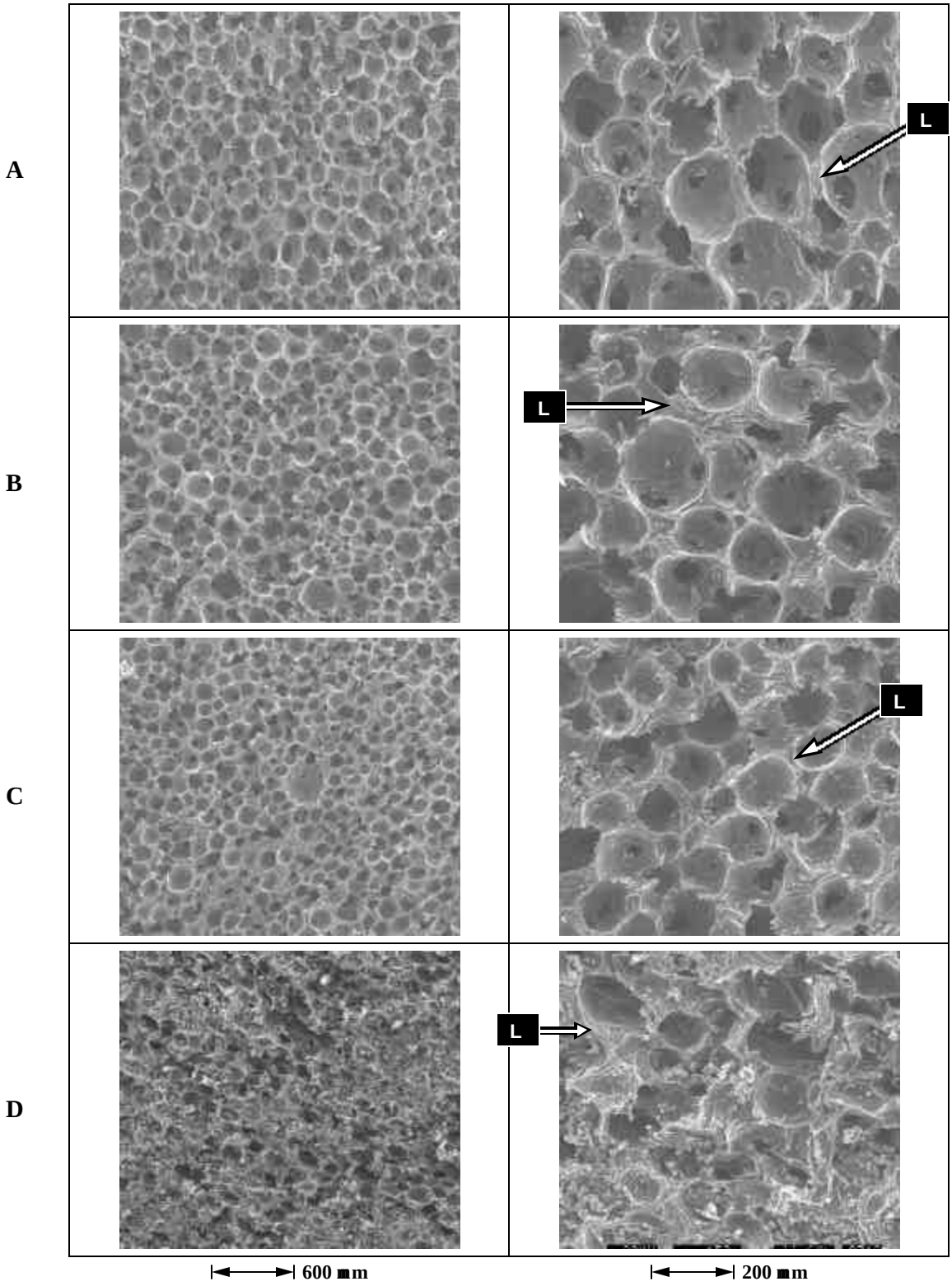

Figure 5. SEM photomicrographs of the foams produced from Conoco Pitch at different densities A < B < C < D (all samples carbonized at 1000°C).

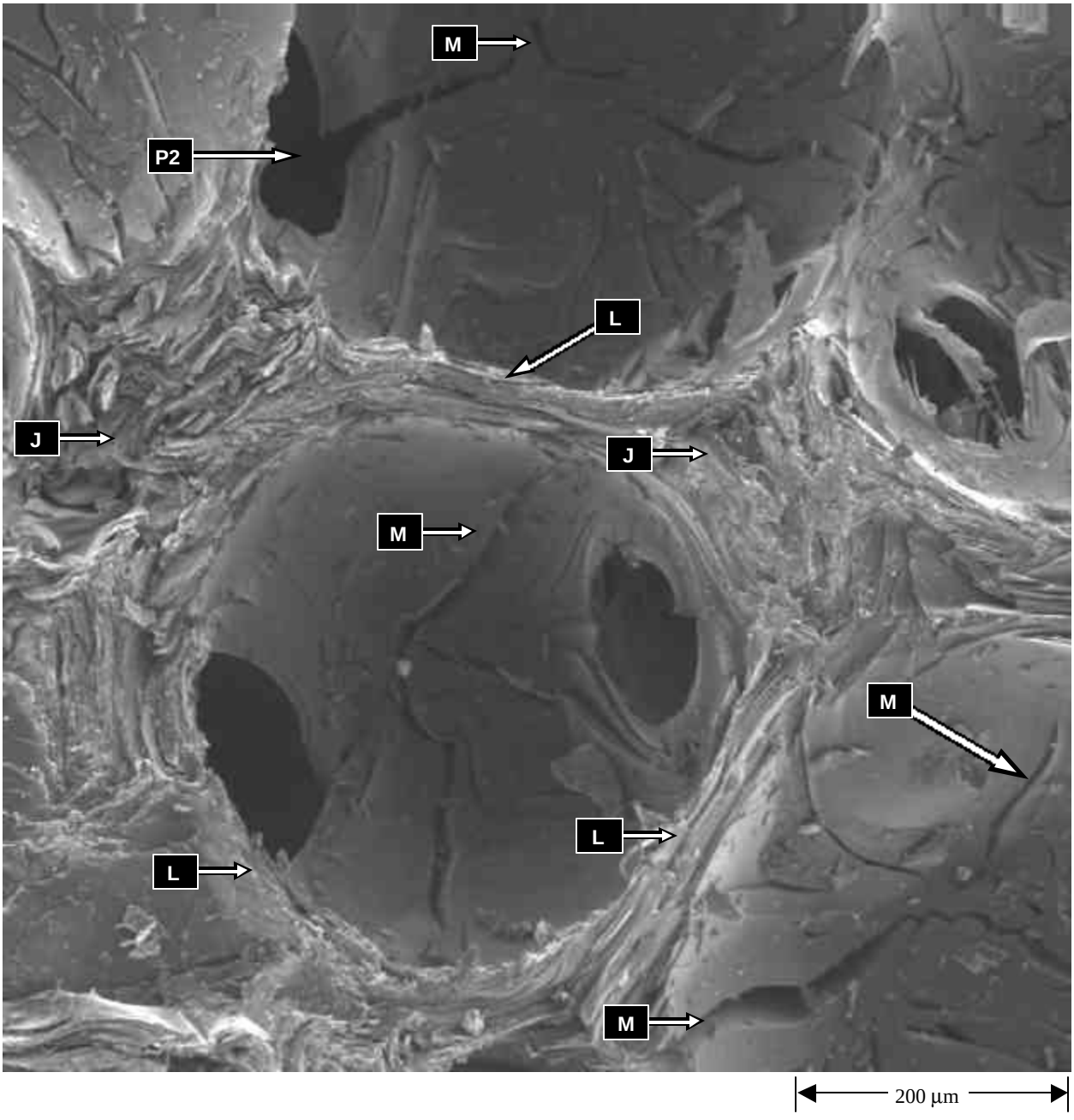

Figure 6. Structure of Mitsubishi ARA pitch-derived carbon foam carbonized at 1000°C.

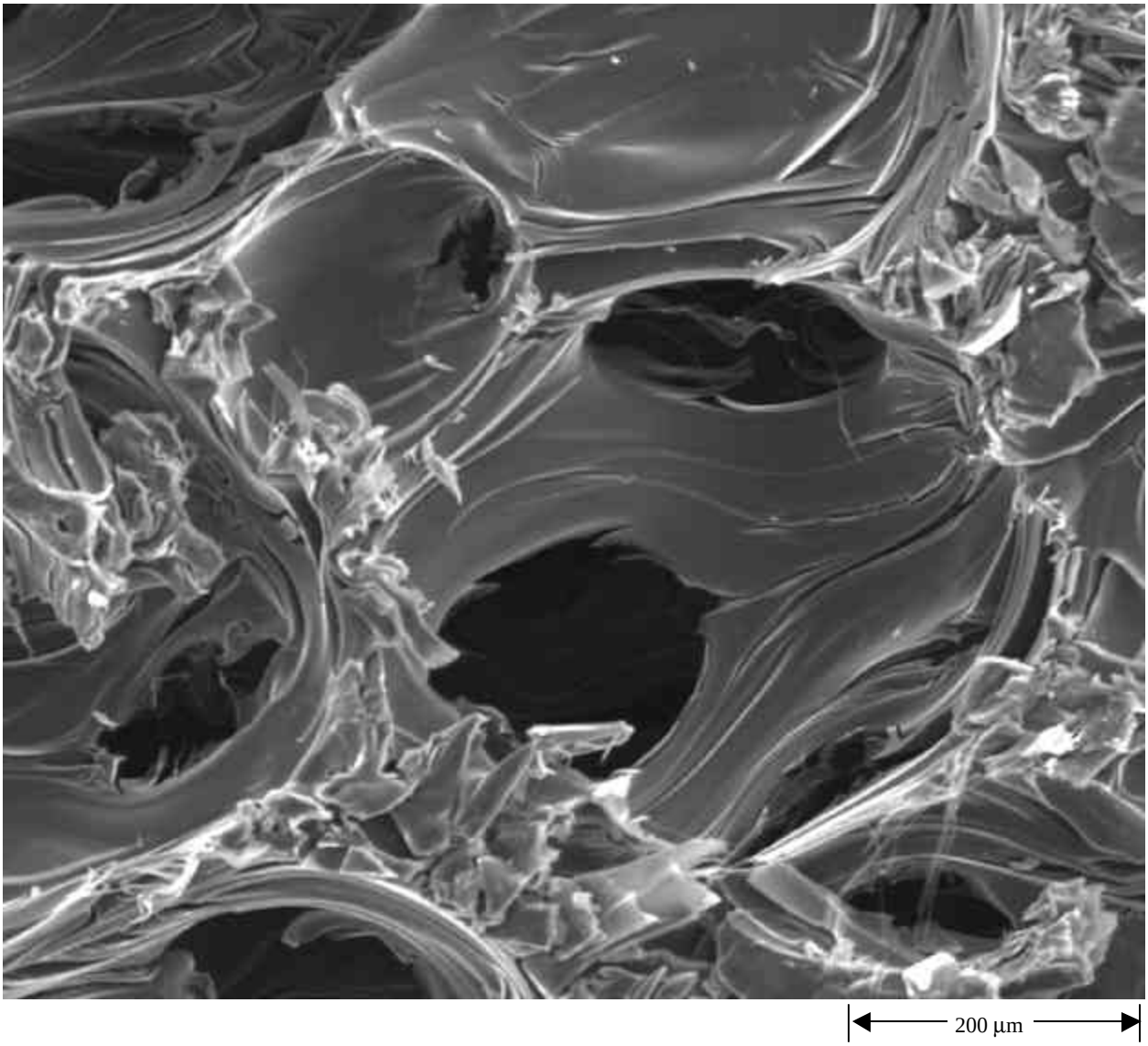

Figure 7. Structure of Mitsubishi ARA pitch-derived carbon foam graphitized at 2800°C.

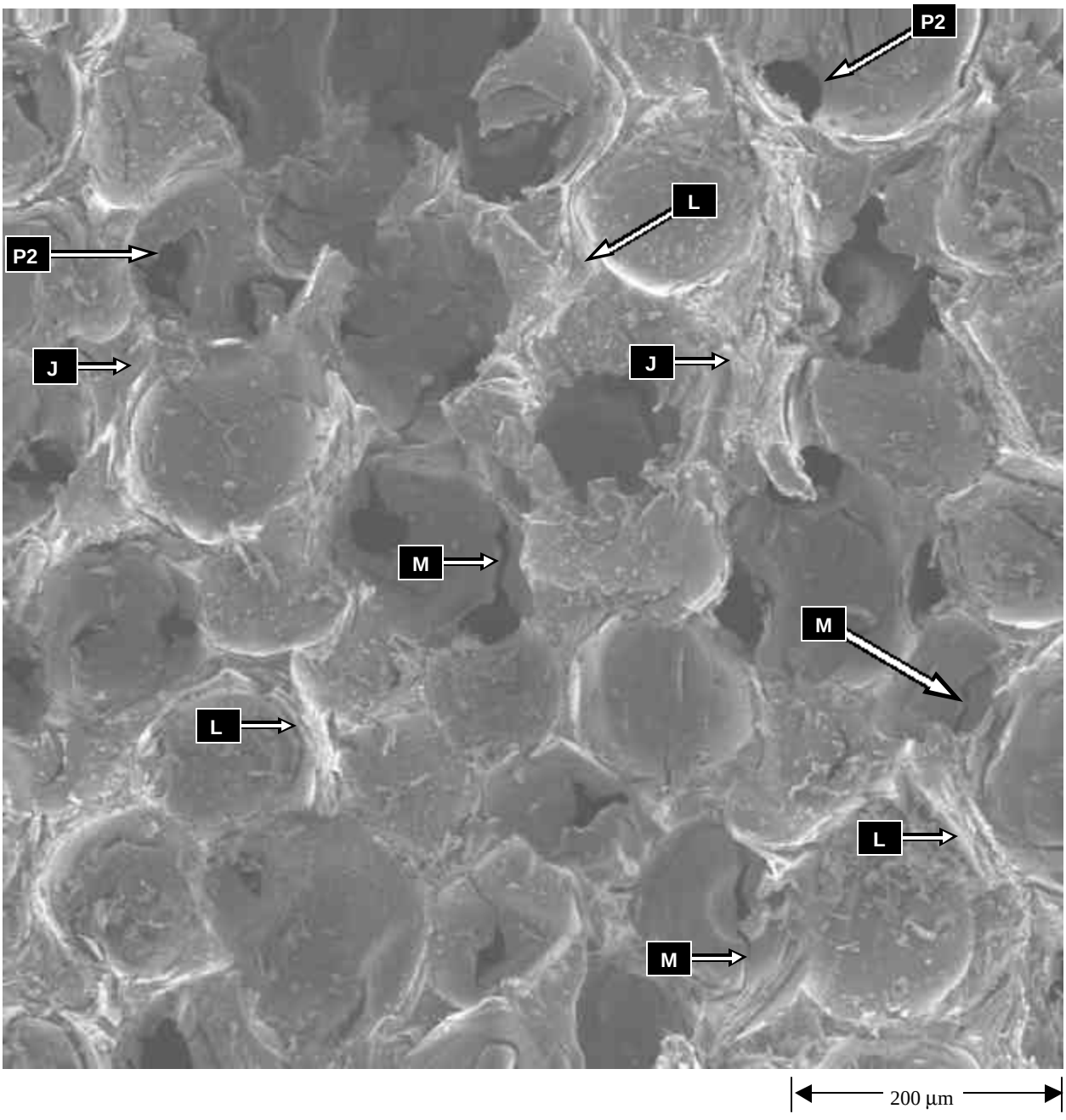

Figure 8. Structure of Conoco pitch-derived carbon foam carbonized at 1000°C.

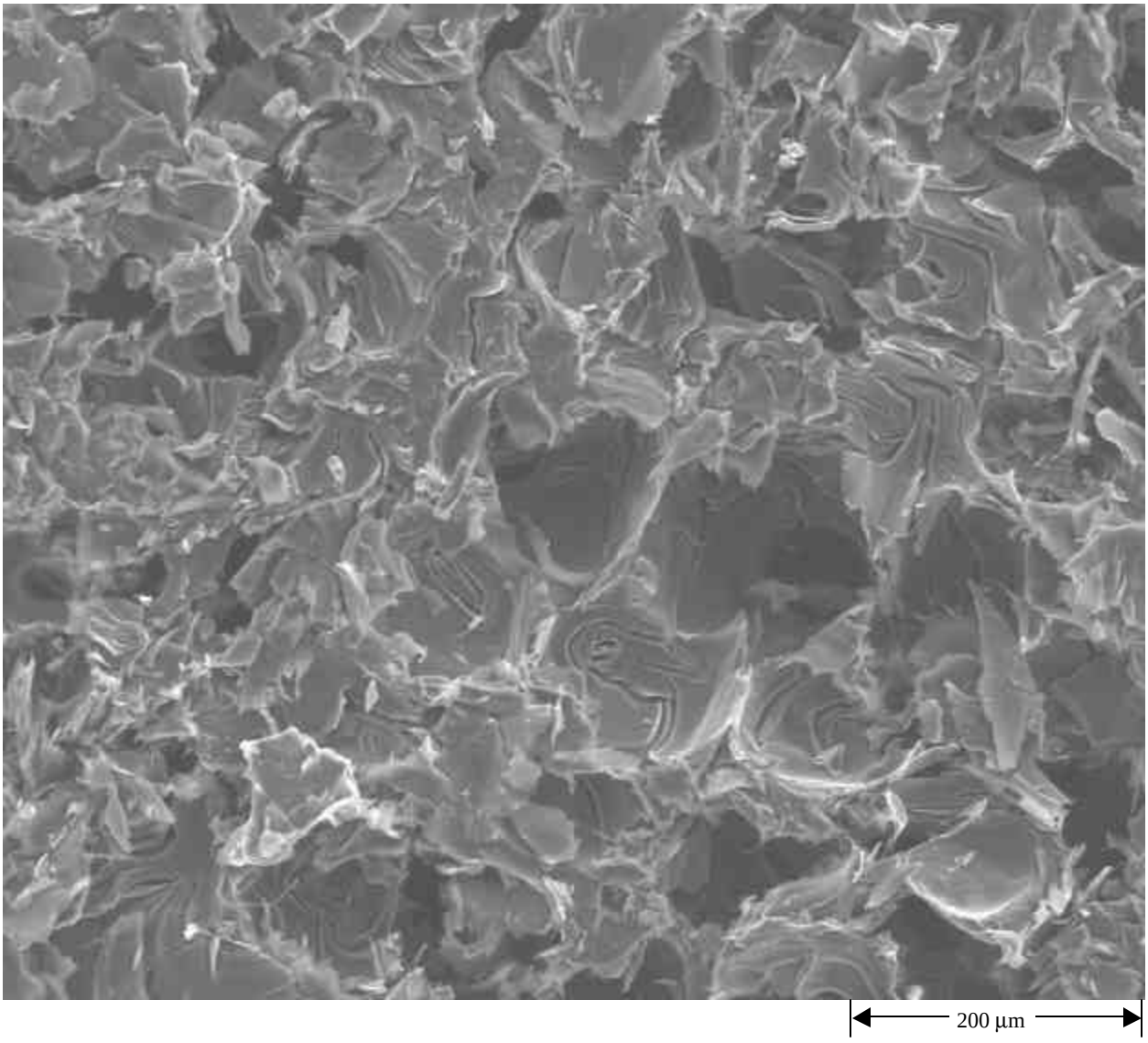

Figure 9. Structure of Conoco pitch-derived carbon foam graphitized at 2800°C.

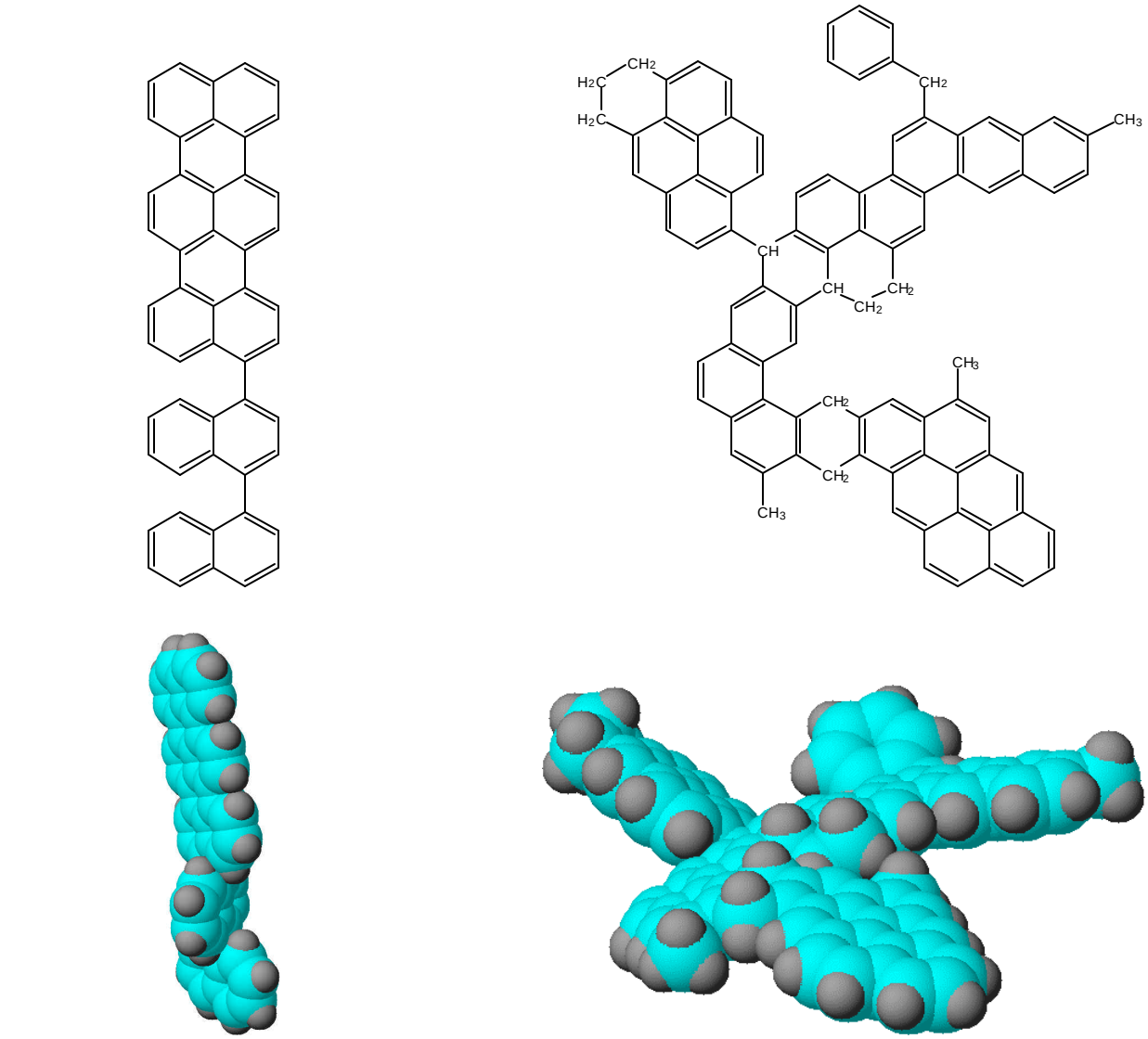

(a) AR Mesophase

(b) Typical Petroleum Mesophase

Figure 10. Representative polynuclear aromatic hydrocarbons found in (a) AR mesophase [26] and (b) typical petroleum mesophase [27].

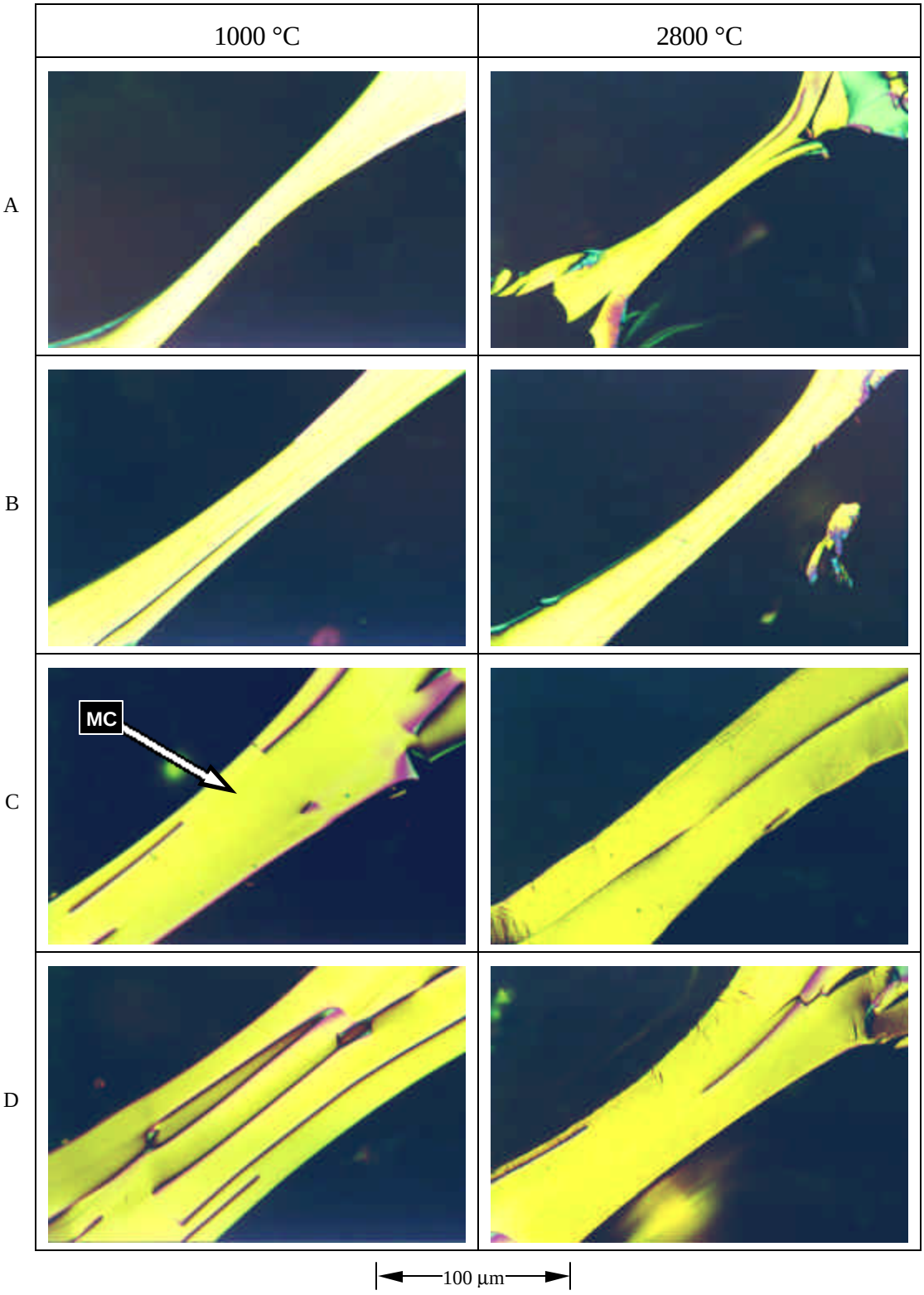

Figure 11. Optical micrographs of ligaments in the ARA24 pitch-derived foam carbonized at 1000°C and graphitized at 2800°C (Densities A < B < C < D).

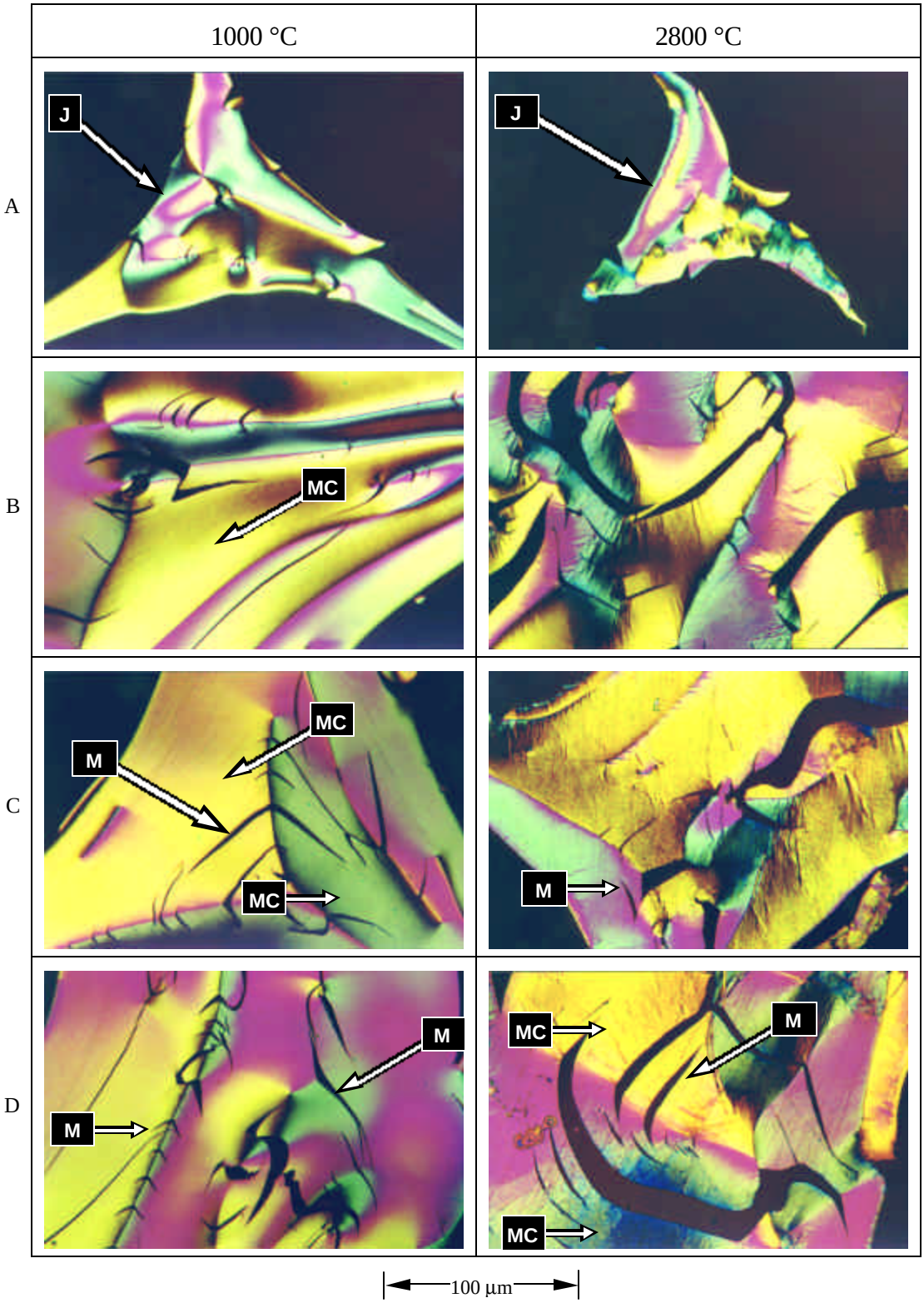

Figure 12. Optical micrographs of junctions in the ARA24 pitch-derived foam carbonized at 1000°C and graphitized at 2800°C (Densities A < B < C < D).

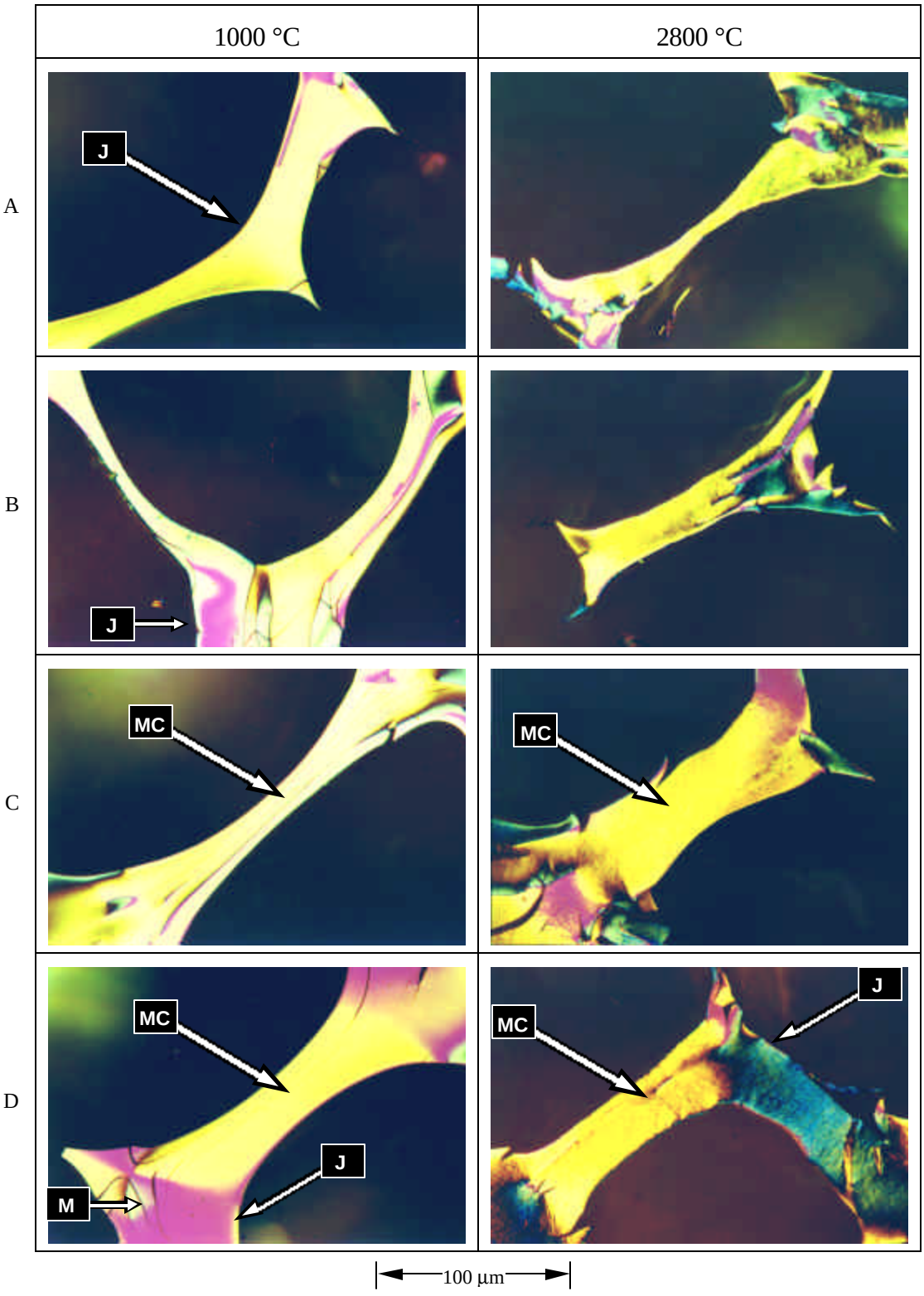

Figure 13. Optical micrographs of ligaments in the Conoco pitch-derived foam carbonized at 1000°C and graphitized at 2800°C (Densities A < B < C < D).

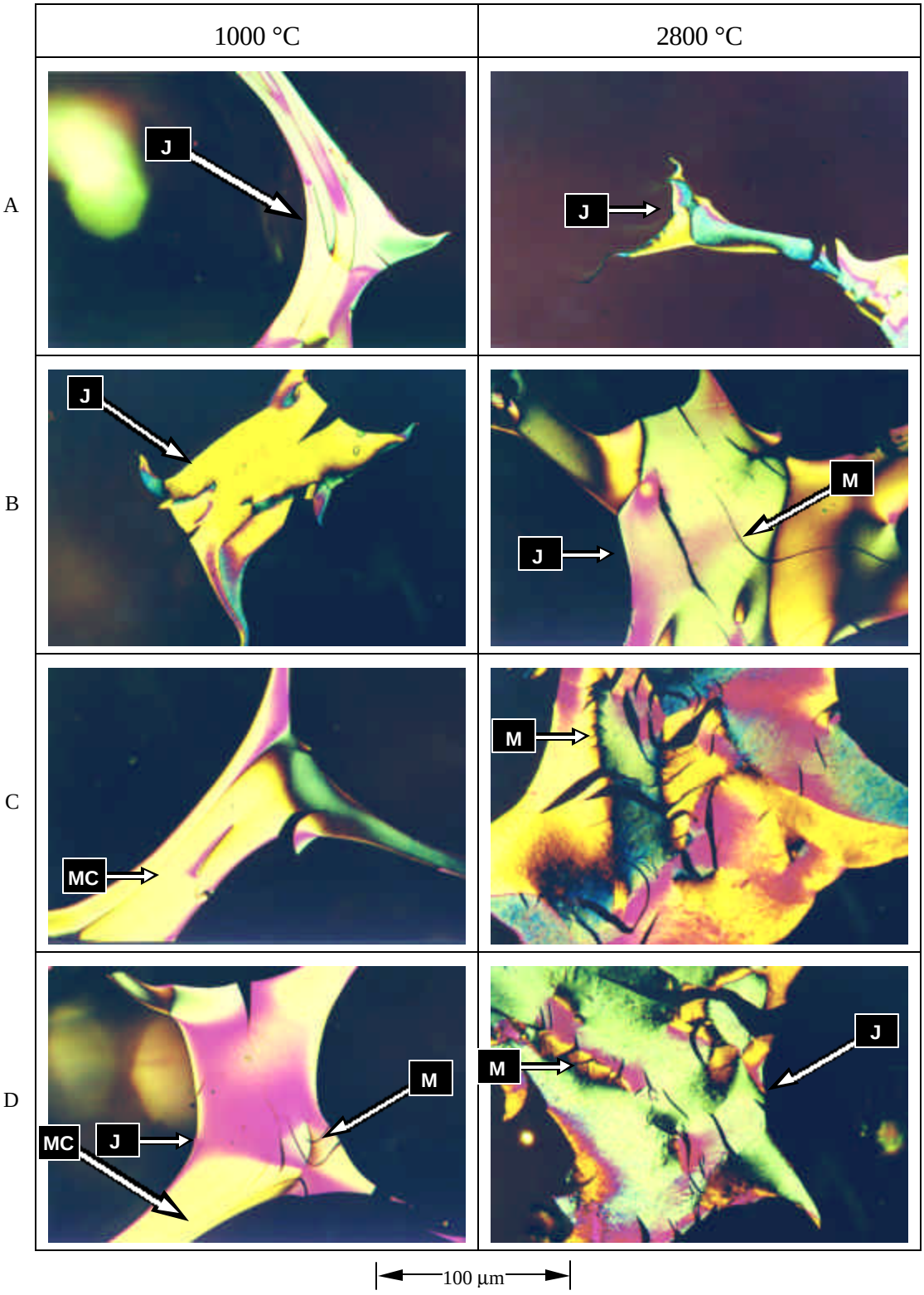

Figure 14. Optical micrographs of junctions in the Conoco pitch-derived foam carbonized at 1000°C and graphitized at 2800°C (Densities A < B < C < D).

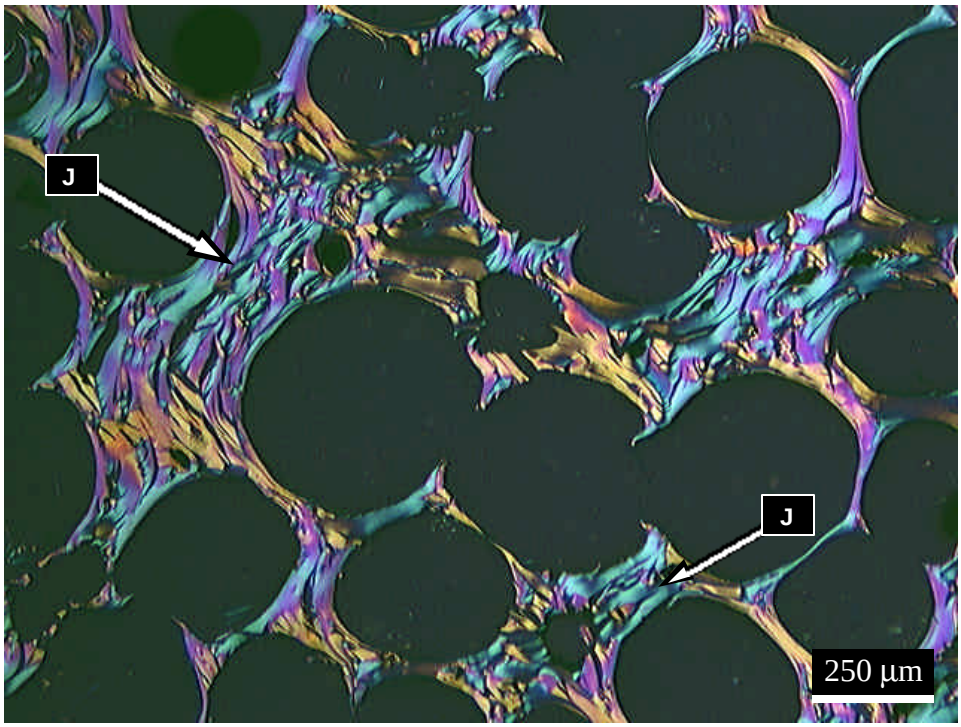

(a)

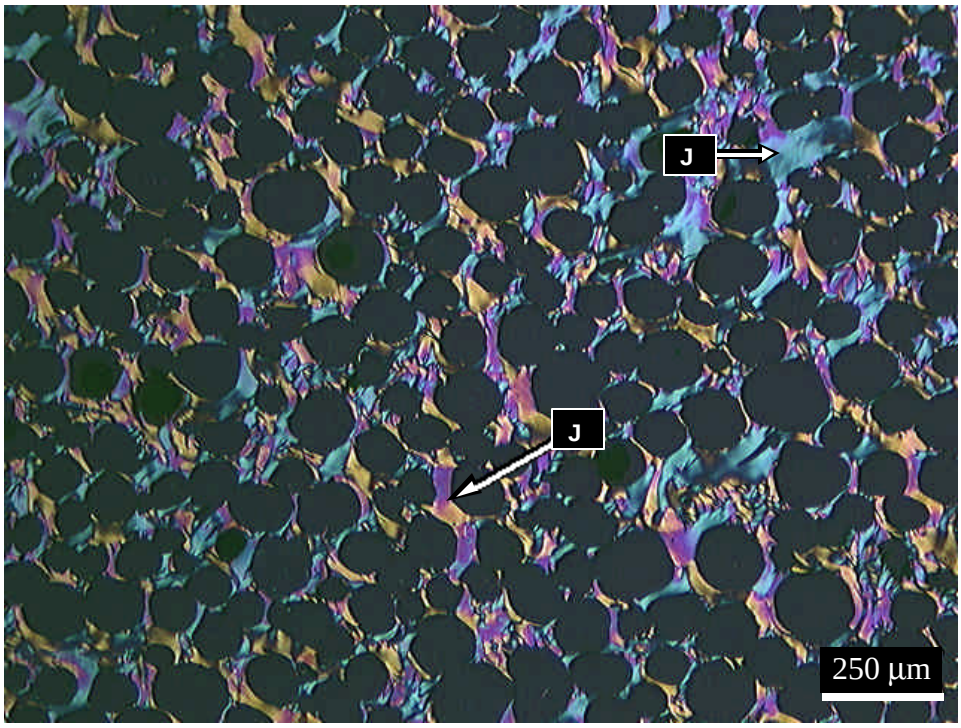

(b)

Figure 15. Comparison of flow texture in junctions between (a) ARA24 and (b) Conoco pitch-derived foams formed with process D graphitized at 2800°C.

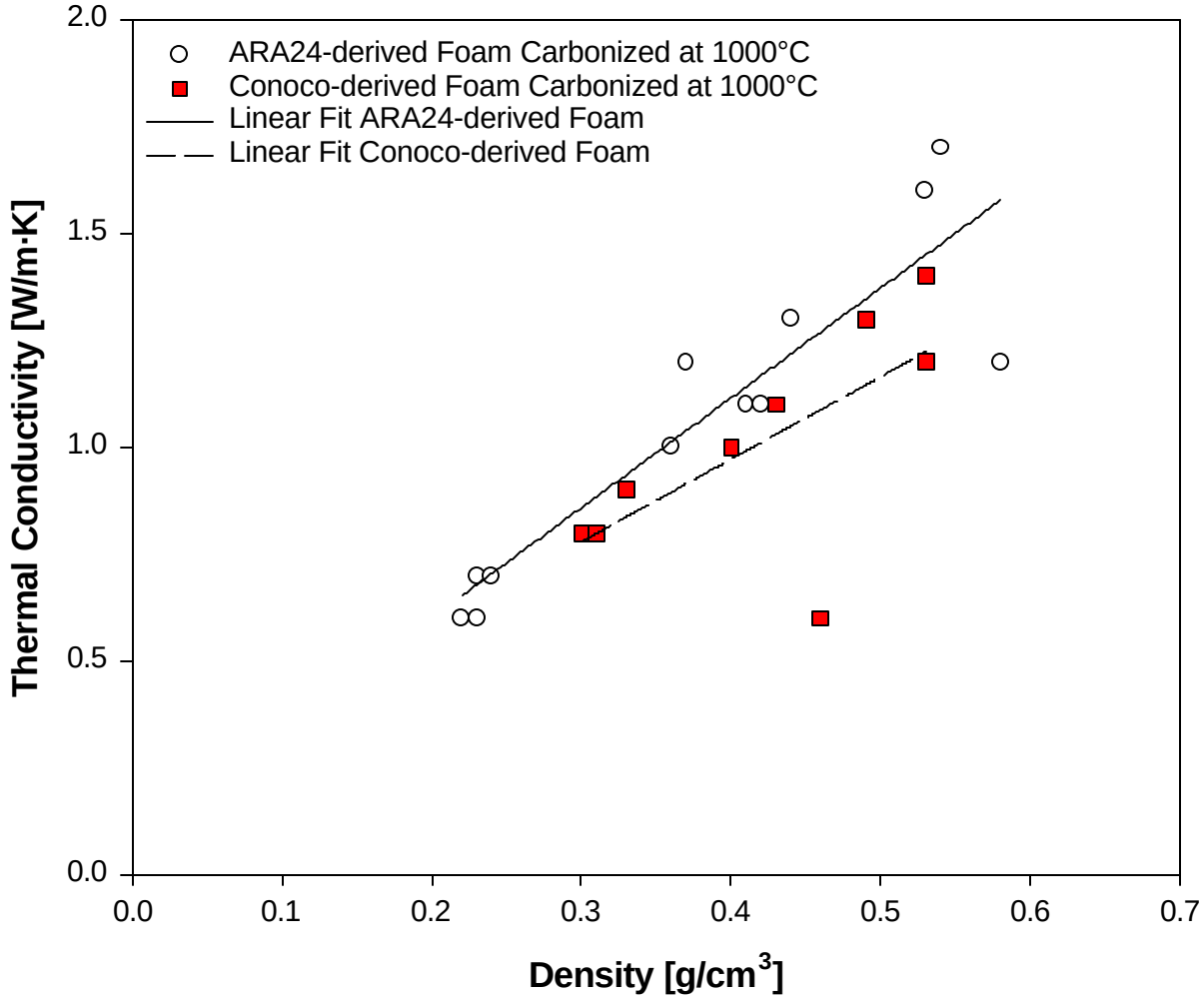

Figure 16. Thermal conductivity as a function of density for ARA Mesophase pitch-derived foams and Conoco-derived foams carbonized at 1000°C.

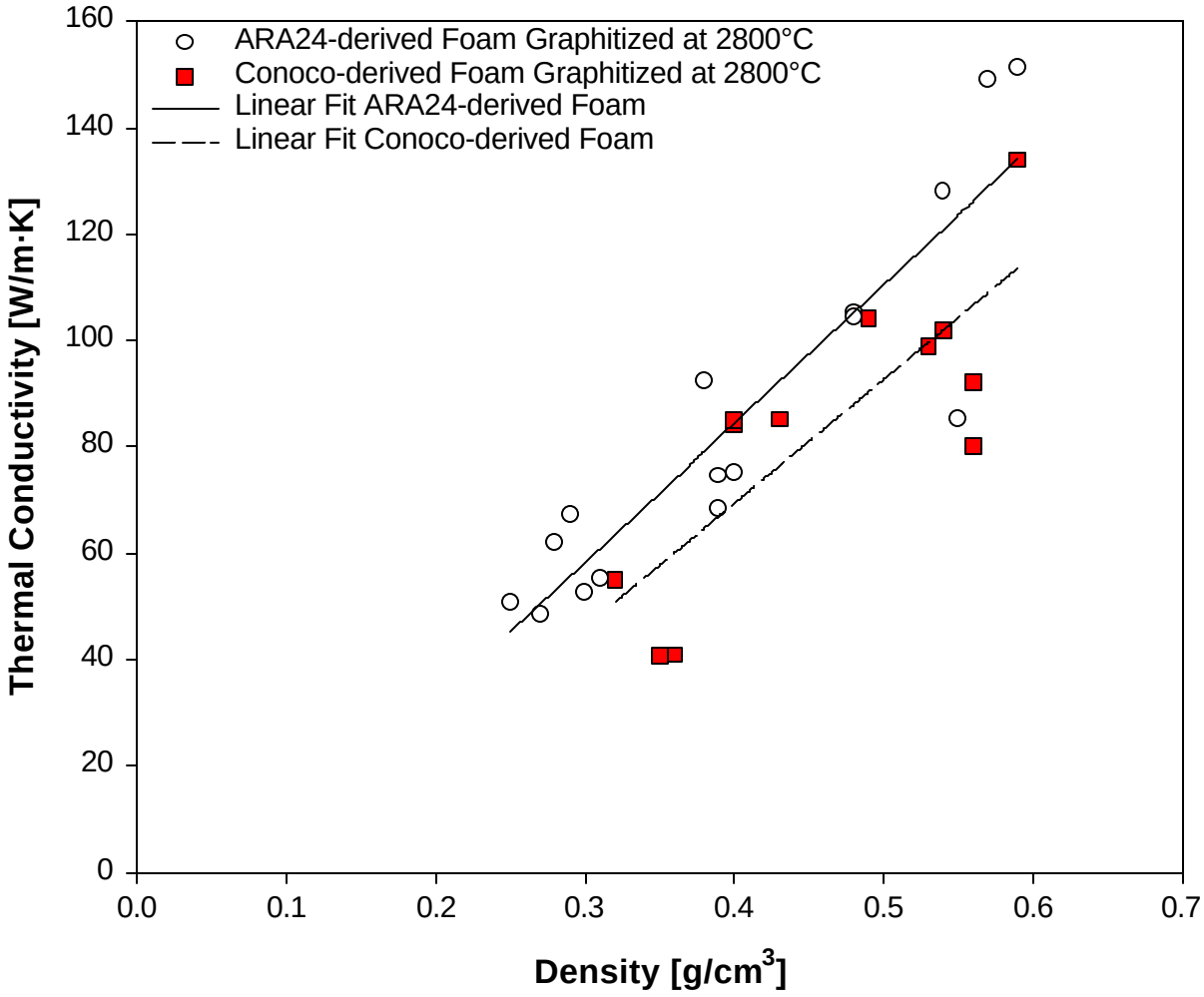

Figure 17. Thermal conductivity as a function of density for ARA Mesophase pitch-derived foams and Conoco-derived foams graphitized at 2800°C.

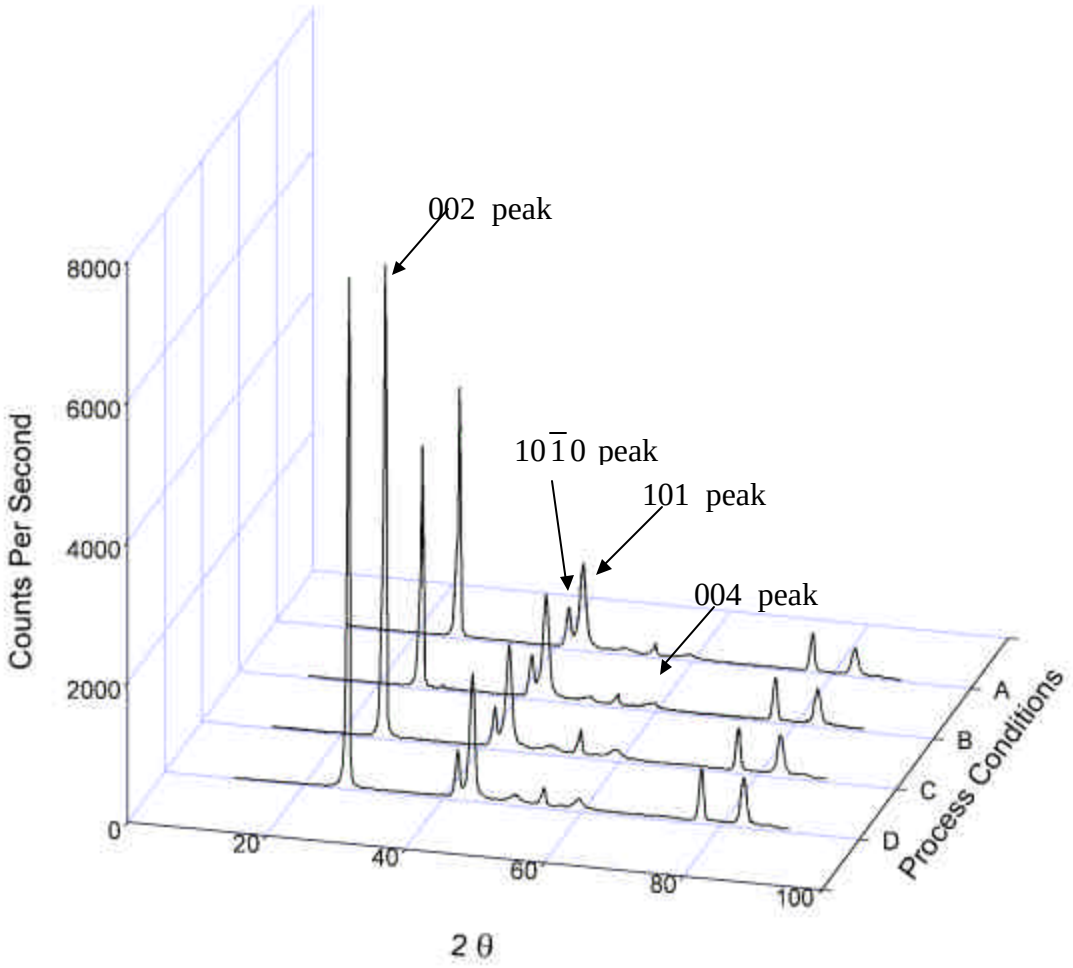

Figure 18. X-ray diffraction patterns of ARA24-derived foams graphtized at 2800°C.

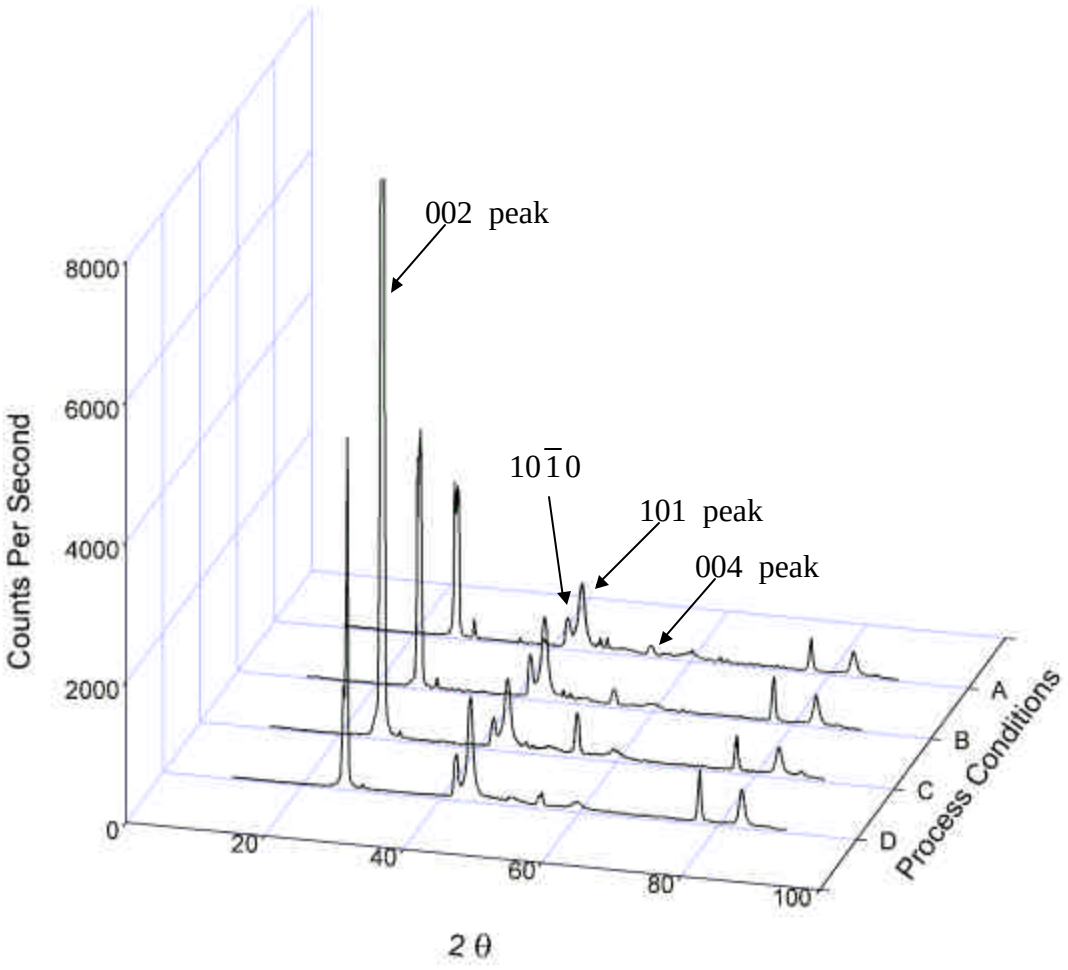

Figure 19. X-ray analysis of Conoco pitch-derived foams graphtized at 2800°C.

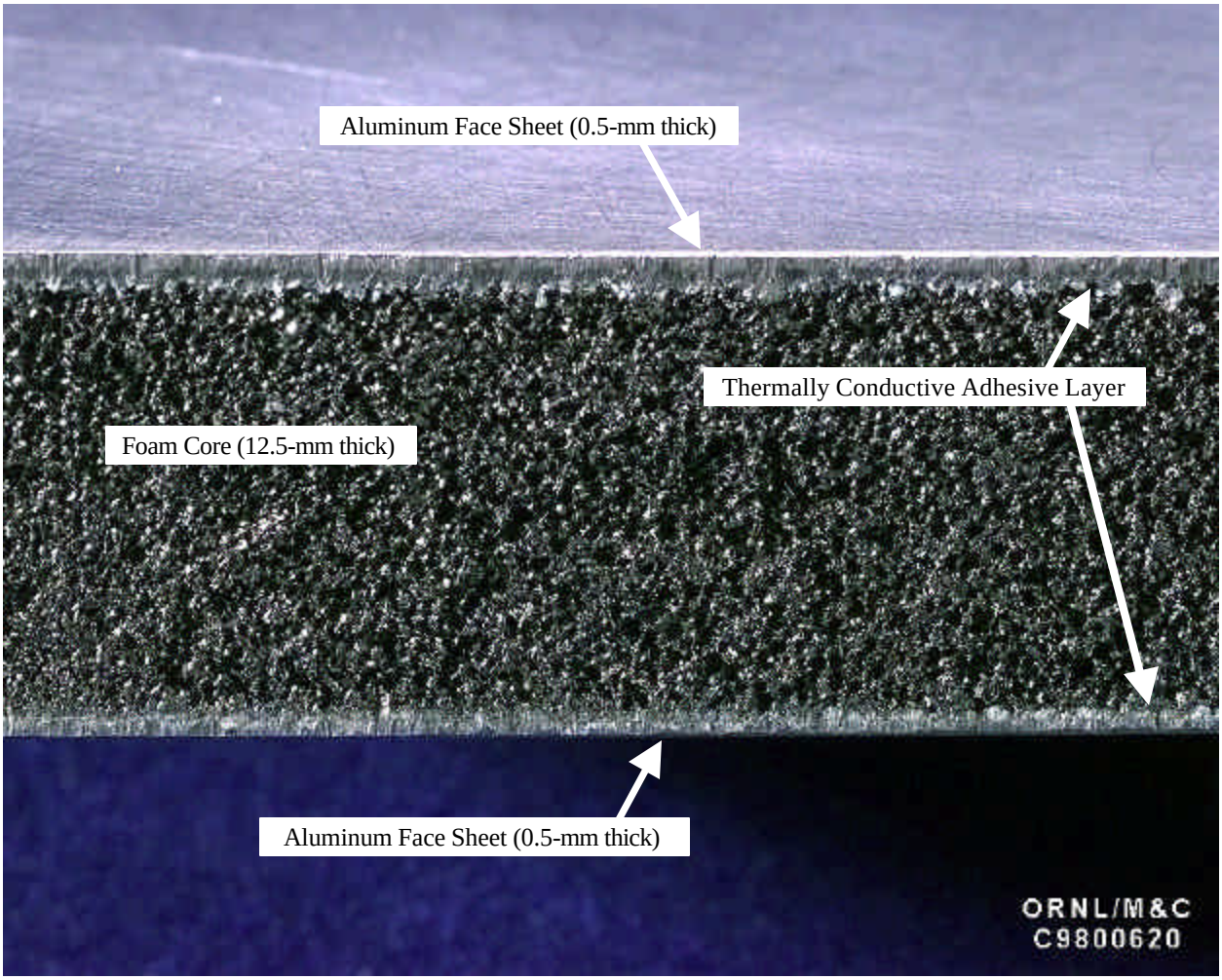

Figure 20. High thermal conductivity foam-core composite with aluminum face sheets.